LITHOS 452-453 (2023) 107227

Contents lists available at ScienceDirect

LITHOS

journal homepage: www.elsevier.com/locate/lithos

Evolution of the Palaeozoic mafic-ultramafic Lizard Complex (SW England) from zircon and baddeleyite U-Pb-Hf isotopic constraints: New thoughts on the convergence of Avalonia and Armorica

Allen P. Nutman[a,*], Vickie C. Bennett[b], David H. Green[c], Clark R.L. Friend[d]

[a] GeoQuEST Research Centre, School of Earth, Atmospheric and Life Sciences, University of Wollongong, Wollongong, NSW 2522, Australia
[b] Research School of Earth Sciences, The Australian National University, Canberra, ACT 2610, Australia
[c] Centre for Ore Deposits and Earth Sciences, University of Tasmania, Hobart, TAS 7001, Australia
[d] Glendale, Tiddington, Oxon OX9 2LQ, UK

ARTICLE INFO

Keywords:
Lizard Complex
Crousa Downs Gabbro
Baddeleyite
Ophiolite
Variscides

ABSTRACT

The Palaeozoic Lizard Complex of southwestern England is composed of a peridotite body with gabbro and intruded by granitic rocks. The peridotites are bounded by amphibolite schists and metasedimentary rocks with those in the southern region also intruded by granodiorite sheets. These granodiorites sheets are coeval with the Man-of-War Gneiss on islets south of the Lizard headland. To the north, the Lizard Complex is in tectonic contact with the Devonian Gramscatho Group.

Zircon and baddeleyite U-Pb-Hf isotopic data and zircon REE chemistry presented here provide more accurate resolution of the Lizard Complex's evolution. The Old Lizard Head Series at the southern point of the Lizard headland is intruded by granodiorite bodies with ages of 488 ± 11 and 499 ± 7 Ma, indistinguishable from the 498 ± 11 Ma age for the Man-of-War Gneiss. Thus the rocks bounding the Lizard Complex are interpreted as a Cambrian (Miaolingian or older) volcano-sedimentary and felsic intrusions package. The inital $\varepsilon Hf_{(498Ma)}$ values of the Man O'War Gneiss zircons range from +8.1 to +9; these values fall below depleted mantle estimates and are indicative of some older crustal components in the source region of the gneisses. The Landewednack and Traboe Hornblende Schists bounding the Lizard Complex carry prismatic oscillatory-zoned zircons that have U-Pb ages of ca. 490 Ma (Cambrian) and are interpreted as volcano-sedimentary in origin. Structureless zircons and rims on oscillatory zircon in these schists have U-Pb ages of 390–370 Ma and are interpreted as metamorphic in origin. The Crousa Downs Gabbro was intruded into the Lizard Complex peridotite at low pressure, and relict baddeleyite in it has a U-Pb age of 416 ± 17 Ma (Lower Devonian). The baddeleyite is variably recrystallised to zircon, and separate zircons have a U-Pb age of 393 ± 11 Ma, interpreted as indicating growth of zircon from igneous baddeleyite recrystallisation. The initial $\varepsilon Hf_{(416\ Ma)}$ of the zircon grains is +13.4 to +15.6, indicating the gabbro has a depleted mantle source, uncontaminated by older continental crust. The new geochronology demonstrates that the Traboe Hornblende Schists are not genetically related to the Crousa Downs Gabbro, as was proposed in some previous studies. Pyroxene granulite felsic intrusions in the margin of the Lizard peridotite have magmatic zircons with U-Pb ages of 384 ± 11 and 396 ± 9 Ma, agreeing with the previously acquired zircon U-Pb ages on the Kennack Gneiss intrusions in the Lizard Complex. The pyroxene granulite magmatic zircon shows a lack of enrichment in the heavy REE, indicative of initial zircon growth in equilibrium with garnet. Like the Kennack Gneisses, these granulite felsic intrusions carry older inherited zircons, showing that by ca. 395 Ma, the Lizard peridotite and the juvenile Crousa Downs Gabbro were tectonically underlain by older quartzo-feldspathic crustal rocks. Early Palaeozoic inherited zircon in one of the pyroxene granulite sheets has an initial εHf value of ~ + 8, similar to the Man O'War Gneiss magmatic zircons.

The new data from the Lizard Complex are compatible with, and provide additional time constraints for previously expressed models that distal to subduction farther south, the Lizard Complex is part of a narrow, short-lived rift that during extension was invaded by a peridotite diapir and then an early Devonian gabbro intrusion. This rift was then inverted by northerly-directed thrusting starting shortly after 400 Ma, as a Normanian terrane thrust-nappe advanced to override progressively the Devonian Gramscatho Group to the north.

* Corresponding author.
E-mail address: anutman@uow.edu.au (A.P. Nutman).

https://doi.org/10.1016/j.lithos.2023.107227
Received 22 February 2023; Received in revised form 17 May 2023; Accepted 20 May 2023
Available online 25 May 2023
0024-4937/

Melting deep in the tectonically thickened crust, at least part in the stability field of garnet, had started by 390 Ma. Thus, although the Lizard Complex has some similarities with ophiolites, it is not the remnant of a broad domain of oceanic lithosphere.

1. Introduction

The Lizard Complex (Figs. 1 and 2) is an allochthonous body of predominantly ultramafic and mafic rocks (Green, 1964a; Vearncombe, 1980; Styles and Kirby, 1980; Cook et al., 2002; Nutman et al., 2001; Leveridge and Shail, 2011), thrust NNW over the upper Palaeozoic sediments in the late Palaeozoic Variscan fold and thrust belt of SW England (e.g., Rattey and Sanderson, 1984; Holder and Leveridge, 1986; Leveridge and Shail, 2011). The Variscan collision, with closure of the Rheic ocean (Cocks and Fortey, 1982, 1990), including emplacement of the Lizard Complex, resulted from the convergence of the southern African continent of Gondwana with the northern continents of Laurentia, Balitica and Avalonia to form the Pangea supercontinent (e.g., Franke, 1989; Murphy et al., 2016; Strachan et al., 2014 and references therein).

Do the peridotites, gabbros and other mafic rocks of the Lizard Complex (~15 × 14 km of the Lizard headland Fig. 2) mark the closure of a Palaeozoic ocean of considerable width and maybe even the main suture marking the disappearance of the Rheic Ocean (e.g. Kirby, 1979)? In this perspective, some workers have regarded the Lizard Complex as a slice of oceanic crust sensu stricto emplaced over continental crust and hence it has been interpreted as an ophiolite (e.g., Bromley, 1975, 1979; Floyd et al., 1993; Kirby, 1979; Styles and Kirby, 1980). Alternatively, does the Lizard Complex mark the closure or a narrow seaway / rift, as one of several closures leading to the demise of the Rheic Ocean (e.g. Franke et al., 2017; Alexander et al., 2019)? Syntheses such as Floyd (1984), Cook et al. (2002) and Leveridge and Shail (2011) proposed that the Lizard Complex is thus part of an early Devonian short-lived rift, which during its opening was invaded by a peridotite diapir and then a gabbro intrusion (the Crousa Downs Gabbro). This rift was then inverted by northerly-directed thrusting starting shortly after 400 Ma, when a thrust-nappe of southern Normanian terrane basement rocks progressively advanced to override the syn-orogenic Devonian Gramscatho Group to the north (e.g., Leveridge and Hartley, 2006; Shail and Leveridge, 2009). Hence, there are several plate tectonic scenarios into

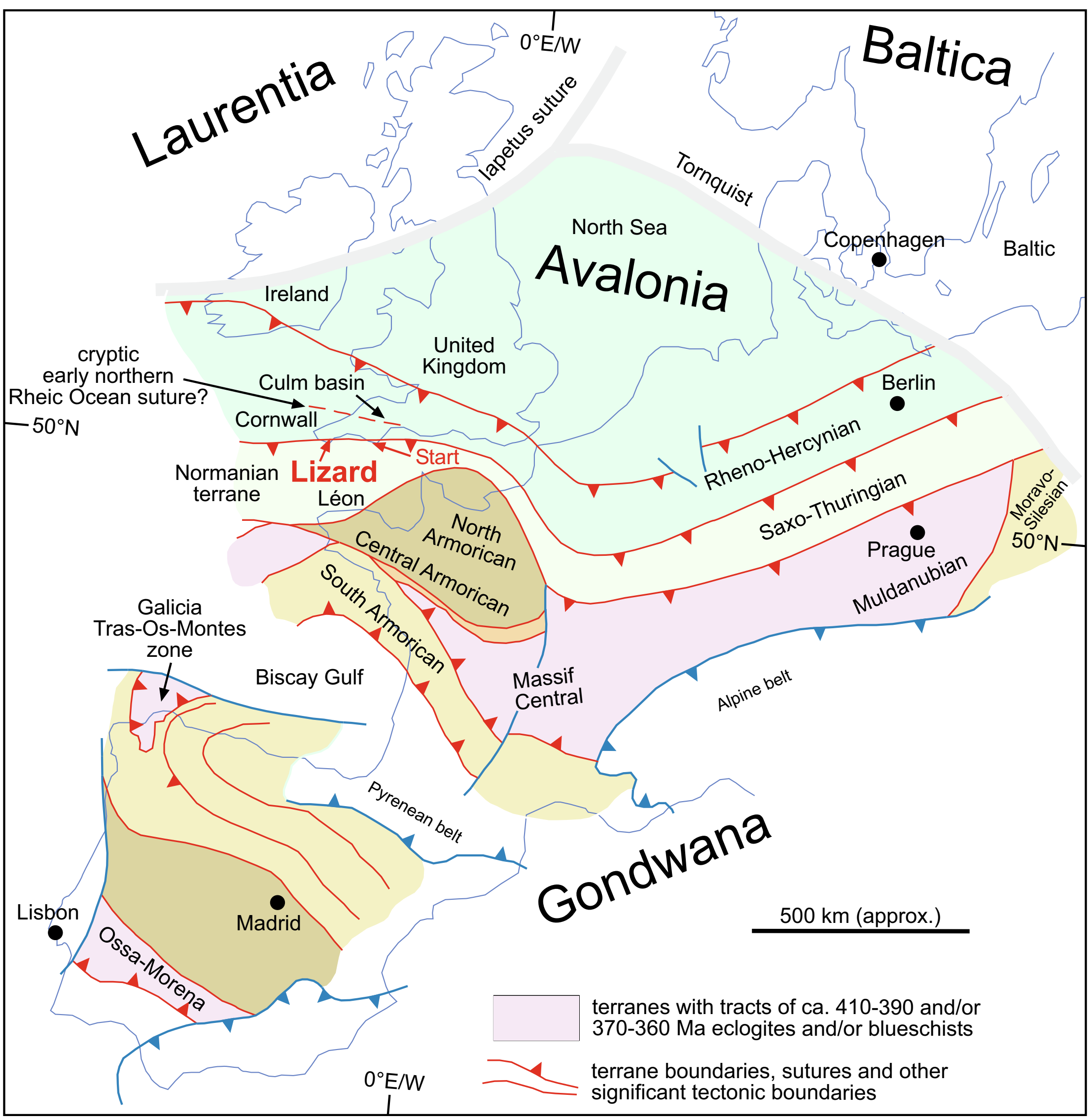

Fig. 1. Tectono-stratigraphic map of Western Europe showing the location of the Lizard Complex (adapted from Fig. 1 of Ballèvre et al., 2009).

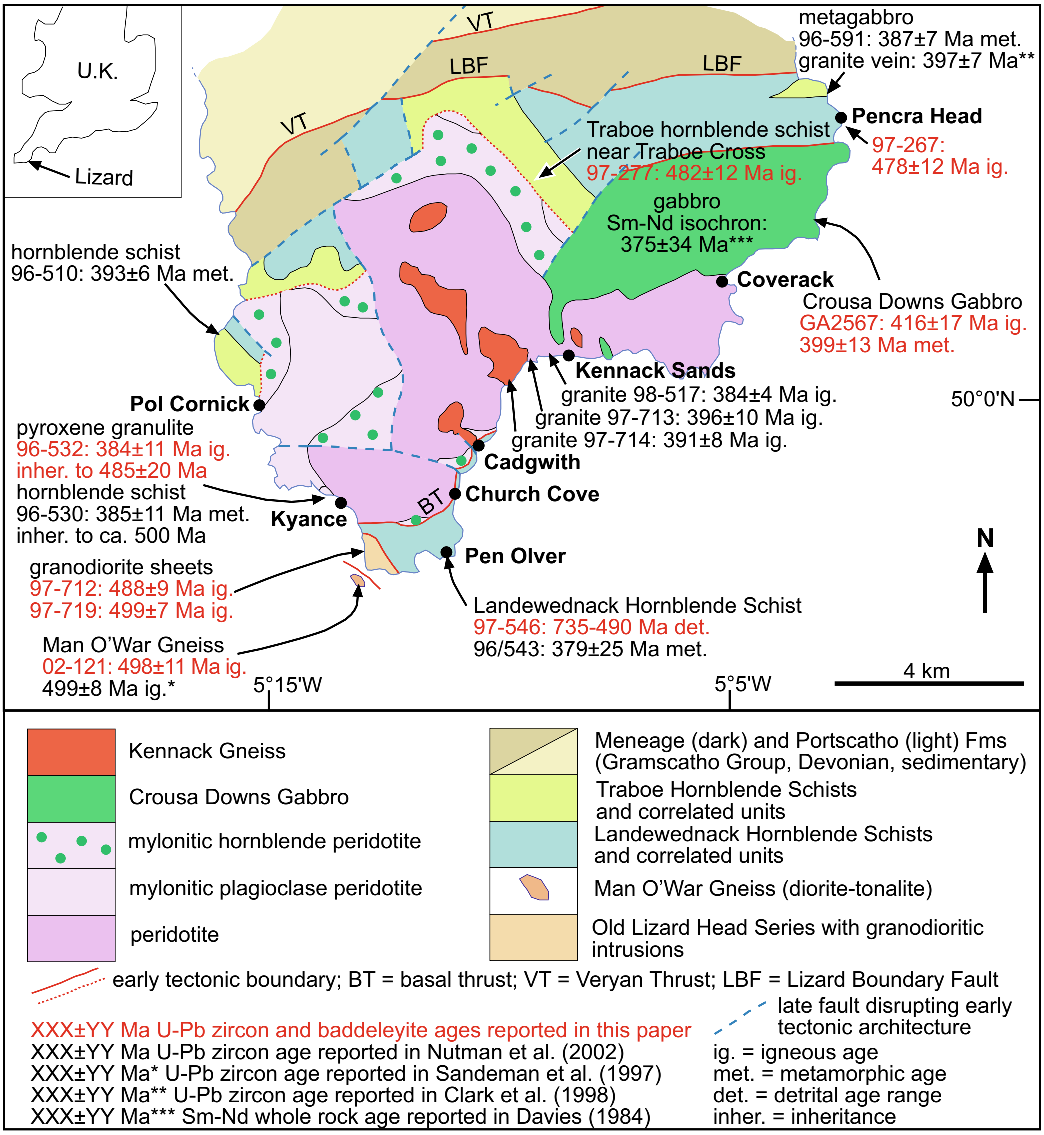

Fig. 2. Geological map of the Lizard Complex (adapted from Fig. 1 of Nutman et al., 2001).

which the Lizard Complex has been placed. Three of these scenarios are illustrated in Fig. 3 (adapted after Fig. 7 in Shail and Leveridge, 2009).

In this paper, to constrain further interpretation of the Lizard Complex, we provide new zircon and baddeleyite U-Th-Hf isotopic and rare earth element (REE) trace element data. This follows a >20 year hiatus (since Sandeman et al., 1997, 2000; Nutman et al., 2001) in presentation of U-Pb zircon age data on the Lizard Complex, for which its geodynamic significance continues to be debated. The new data fit better with models of inversion of a Devonian rift (probably narrow) invaded by a peridotite diapir, rather than closure of an extensive ocean (e.g., Floyd, 1984; Cook et al., 2002; Leveridge and Shail, 2011). On a broader scale, the new age data add constraints on events in the evolution of the Palaeozoic Variscan orogen (Europe). In particular, the new results further support, as recently reviewed by Franke et al. (2017), that the "one ocean" model for the Variscides should be discarded.

2. Geology of the Lizard Complex

2.1. General setting

The Lizard Complex occupies ~15 × 14 km of the Lizard headland (Figs. 1 and 2). It marks the southern edge of the Variscan fold and thrust belt in southwest England and is allochthonous to the Devonian Gramscatho Group to the north. The dominant rocks in the Lizard Complex are the Lizard Peridotite and the Crousa Downs Gabbro, which are intruded by felsic bodies such as the ~390 Ma Kennack Gneiss (e.g., Barnes and Andrews, 1984; Bromley, 1975). The peridotite and Crousa Downs Gabbro are bounded by hornblende-bearing schists intruded by granodioritic bodies and on islets to the south, the Man O'War Gneiss (e.g., Sandeman et al., 1997). 2–3 decades ago, zircon U-Pb geochronology provided tighter constraints on the evolution of the Lizard Complex. Thus, Sandeman et al. (1997) reported a 499^{+8}_{-3} Ma protolith age for the Man-of-War Gneiss. Also, Nutman et al. (2001) provided ~390 Ma magmatic ages for the Kennack Gneiss, and identified in them Precambrian inherited zircon cores, as a robust indication that the Lizard Complex is allochthonous over 'fertile' quartzo-feldspathic rocks which melted to generate the Kennack Gneiss. Previously, Davies (1984) provided a Sm-Nd mineral isochron age of 375 ± 34 Ma for the Crousa Downs Gabbro, which is a *minimum* age for the gabbro's magmatic emplacement. The Variscan emplacement is expressed in the Carne Formation and Roseland Breccia Formation (formerly Meneage), dipping southward under the Lizard Complex and exposed on the east coast of the Lizard Peninsula (e.g., Leveridge and Shail, 2011; Strachan et al., 2014).

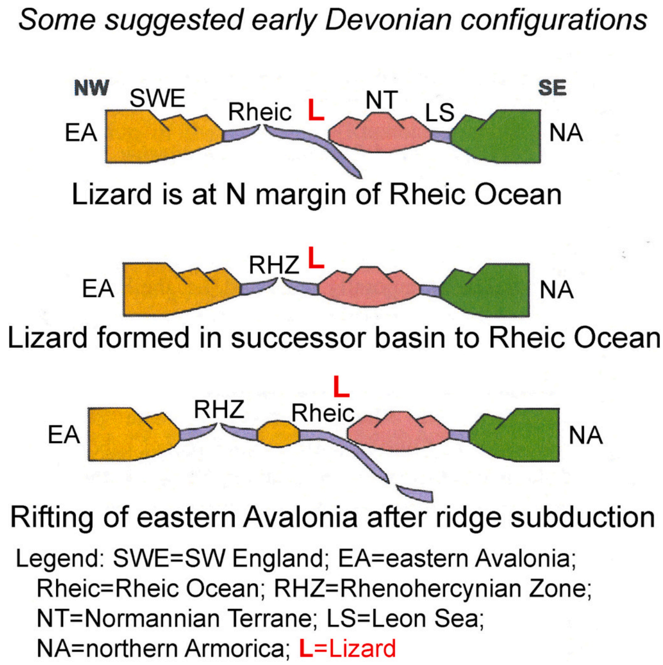

Fig. 3. Some proposed early Devonian syntheses showing the location of the Lizard Complex between SW England, various basins and the Normanian Terrane (adapted from Fig. 7. in Shail and Leveridge, 2009).

The Lizard Peninsula is divided into three tectonic units (Bromley, 1979): (1) Basal Unit with the Man-of-War Gneiss (structurally lowest); (2) Rocks of the Lizard Complex (dominated by the Lizard Peridotite) and (3) Devonian sedimentary and volcanic rocks of the Gramscatho Group (Fig. 2). These were juxtaposed along thrust faults during NNW-directed Variscan convergence. A granite, the Kennack Granite and Gneiss (e.g., Sandeman et al., 2000) intrudes the Lizard Complex and has been commonly assumed to be sourced below the Basal Thrust and to cut it (e.g., Green, 1964b; Sandeman et al., 2000). Direct evidence for this comes from Precambrian inherited cores within Kennack Gneiss ~390 Ma magmatic zircon (Nutman et al., 2001).

There is excellent exposure along the rocky coastline, where detailed relationships between lithologies can be documented (e.g., Cook et al., 2002; Green, 1964b). However, inland the exposure is very limited and boundaries between lithologies are rarely observed. Interpretation of the geology inland is further complicated by the late sub-vertical faults that disrupt the earlier tectono-stratigraphy related to compressional deformation such as the basal thrust under the Lizard peridotite (Cook et al., 2002 and references therein) and the following extensional dislocations such as the reactivated boundary between the Lizard Complex and the footwall Devonian sedimentary rocks of the Meneage Formation to the north (e.g., Leveridge and Shail, 2011).

2.2. Man-of-War Gneiss, Old Lizard Head Series and Landewednack Hornblende Schists

Flett and Hill (1912) and Green (1964c) suggested that the oldest units on the Lizard are the Old Lizard Head Series, the Man-of-War Gneiss, and the Landewednack Hornblende Schists (Fig. 2). The Old Lizard Head Series are metasedimentary rocks dominated by mica schists, garnet mica schists and hornblende mica schists, which variably contain cordierite, anthophyllite, andalusite, staurolite, kyanite and sillimanite (Flett, 1946; Tilley, 1937). Granodioritic layers interpreted as intrusive sills or as lava flows in the Old Lizard Head Series have a U-Pb magmatic zircon age of ~500 Ma (this paper). The Old Lizard Head Series generally underlies the Landewednack Hornblende Schists at Lizard Point, and there is evidence of thrusting at or near their contact (Fig. 2; Jones, 1994).

The dominant layered amphibolites of the Landewednack Hornblende Schist are interpreted as derived from mafic volcanic rocks and tuffs whilst lesser amounts of (locally discordant) massive amphibolites were derived from doleritic dykes (Floyd et al., 1993; Jones, 1997). The Landewednack Hornblende Schist ~500 Ma age from volcanogenic zircons (this paper) is highly significant, because unlike as suggested for example by Power et al. (1996), these rocks cannot considered as an integral part of a dismembered variably deformed ophiolite assemblage along with the Crousa Downs Gabbro, which is ~100 million years younger (Davies, 1984; this paper).

The Man-of-War Gneiss, on reefs south of Lizard Head (Fig. 2), includes igneous-textured dioritic and tonalitic rocks, and foliated tonalite and quartzo-feldspathic gneiss (Flett, 1946; Sandeman et al., 1997). It has a magmatic zircon age of ~500 Ma (Sandeman et al., 1997; this paper), matching in age the granodioritic sheets in the Old Lizard Head Series. Geochronology also shows that the two granodioritic bodies [6945 1154] in the Old Lizard Head Series have ages of 490 +/− 7 and 488 +/− 9 Ma (95% confidence, MSWDs,1.0), similar to Sandeman et al. (1997) date on the nearby Man-of-War Gneiss.

2.3. Lizard Peridotite

The Lizard Peridotite (Fig. 2) is dominated by partially serpentinised lherzolite. It has a coarse-grained core with a relict high pressure, high temperature ‘primary’ assemblage of:

olivine + aluminous enstatite + aluminous diopside + aluminous spinel (Green, 1964a).

This assemblage has discontinuous layers and lenses relatively enriched in pyroxene and olivine and locally has sharply-bounded layers of serpentinised spinel-bearing dunite. The attitudes of the layering in the lherzolite varies on a km-scale throughout the Lizard (Green, 1964b, 1964c). Geothermometry and barometry applied to the ‘primary’ assemblage indicates 1200 °C and 15 kbar (Cook et al., 2000).

The ‘primary’ assemblage transitions with increasing recrystallisation and grain-size reduction into lherzolite tectonite, in which relict augen of deformed (high pressure) aluminous enstatite and aluminous diopside occur with recrystallised olivine, low-alumina enstatite and diopside, altered plagioclase and spinel (Cook et al., 1998; Green, 1964a). The aluminous spinel is surrounded by rims of altered plagioclase, to demonstrate that deformation and partial recrystallisation of the 15 kbar, 1200 °C assemblage occurred at >10 kbar and ca. 900 °C, and was continuous to <10 kbar, sequentially crossing the reactions:

aluminous pyroxenes + olivine –> aluminous spinel + less aluminous pyroxenes

(decreasing T) and,

pyroxenes + aluminous spinel –> olivine + plagioclase + chromite (decreasing P,T).

The intensity of recrystallisation and grain size reduction increases towards the margins of the Lizard Peridotite. In all marginal areas relict orthopyroxene augen and stringers of spinel can be observed, establishing a link with the precursor high pressure 'primary' assemblage (Green, 1964a, 1964c). Within the recrystallised peridotite tectonite, colourless to pale green pargasitic hornblende is common and can form up to 30% of the lherzolite (Flett, 1946; Green, 1964a). The foliation and intense recrystallisation of the Lizard Peridotite are generally steeply dipping with a NNW-SSE strike and mineral lineations plunge mainly down-dip. An exception to this are the most northerly, inland exposures, where foliations are variable from steep to shallow dipping (Green, 1964b).

2.4. *Traboe hornblende Schists*

The mafic rocks between the peridotite tectonites and the Landewednack Hornblende Schists have been distinguished as the Traboe Hornblende Schists (Flett and Hill, 1912; Green, 1964b; Leake and Styles, 1984; Styles and Kirby, 1980; Vearncombe, 1980). These have compositional layering, granoblastic to lepidoblastic texture, subvertical foliation (commonly with complex refolded folds with steeply-dipping axial planes) and vary from green-brown hornblende + diopside + plagioclase + ilmenite amphibolite through brown hornblende + hypersthene + augite + plagioclase + ilmenite granulite to olivine + hypersthene + augite + plagioclase granulite (Green, 1964b).

2.5. *Crousa Downs Gabbro*

Between along the coast between Church Cove and Coverack (Fig. 2), the peridotite is cut by small bodies of gabbro, usually very coarse-grained and lacking chilled margins (Floyd et al., 1993; Green, 1964c). At Coverack, dykes of troctolite precede the gabbro bodies and cut layering in the lherzolite. North and west of Coverack, the gabbro forms a large body known as the Crousa Downs Gabbro (Fig. 2). Locally the gabbros are intensely deformed into a flaser texture. Olivine coexisting with plagioclase within the troctolite and gabbro demonstrates that their emplacement occurred at low pressure, following most decompression of the peridotite, but when ambient temperatures were still high and there was localized ductile deformation (Green, 1964c).

2.6. *Post-Peridotite emplacement composite mafic-felsic intrusions - the Kennack Gneiss*

Subvertical amphibolitised mafic sheets are exposed in cliffs between Cadgwith and Kennack Sands (Fig. 2). The amphibolite sheets contain interlayered acidic material - the Kennack Gneiss, interpreted as granitic injection gneisses (Green, 1964c). The field relationships show that the granitic veins post-date the mafic components, but suggest that there was little time difference, or that the gently-dipping sheets of dolerite provided a preferred pathway for emplacement, during a thrusting regime, of acid magma. From near Kennack Sands and extending NW, large bodies of medium to coarse grained granite occur within the peridotite, but poor outcrop prevents evaluation of the relative proportions of the contrasted rock types. Sandeman et al. (2000) reported an ID-TIMS U-Pb zircon concordia intercept age of 376.4 ± 1.7 Ma for Kennack Gneiss, whereas using SHRIMP Nutman et al. (2001) reported U-Pb zircon ages of 395–385 Ma for 3 Kennack Gneiss samples and the presence of inherited Precambrian zircon cores. The ≥10 m.y. discrepancy between the magmatic ages proposed in these publications, with related detailed discussions of contrasting analytical techniques and exploring alternative assessments of the data, are discussed in detail in the Clark et al. (2003) comment with the reply by Nutman and co-workers. These ages provide constraint on timing of the tectonic emplacement of the Lizard Peridotite to be before 395 Ma (middle Devonian (Eifelian)) and demonstrate that it is underlain by older continental rocks.

2.7. *Tectonic evolution post formation of the Lizard Peridotite and the Crousa Downs Gabbro*

Many contacts between different lithologies are tectonic, and formed in events spanning from Devonian basin inversion to Permo-Carboniferous late Variscan extension (e.g., Shail and Leveridge, 2009; Leveridge and Shail, 2011; and references therein). At Lizard Head, the Old Lizard Head Series with the intrusions whose magmatic emplacement was coeval with the ca. 500 Ma Man-of-War Gneiss are interpreted to structurally underlie a unit of Landewednack Hornblende Schist, probably separated by a thrust (Fig. 2; Jones, 1997). To the north, the Landewednack Hornblende Schist unit around Lizard Head is in tectonic contact with the Lizard Peridotite. Many of these contacts are later faults, but around Cadgwith (Fig. 2) detailed mapping by Cook et al. (2002) demonstrates that the Landewednack Hornblende Schists are bounded upwards by a sub-horizontal fault, above which is mylonitic peridotite and then coarse-grained lherzolite. This indicates that around Lizard Head the Lizard Complex forms the hanging wall to units of both Landewednack Hornblende Schist and the Old Lizard Head Series. Furthermore, Cook et al. (2002) demonstrated that at Cadgwith the basal tectonic contact of the Lizard Peridotite is cut by a Kennack Gneiss intrusion, indicating the original tectonic contact is pre- ca. 395 Ma.

The north side of the Lizard peridotite and the Crousa Downs Gabbro is in tectonic contact with hornblende schists assigned to both the Traboe and Landewednack units (Fig. 2). There is tectonic partitioning is by earlier approximately east-west trending extensional faults which are displaced by later subvertical faults. The northern of the extensional faults marks the northern limit of the Lizard Complex, against the structurally underlying Devonian Meneage formation with olistostromal components as part of the Gramscatho Group (e.g., Shail and Leveridge, 2009; Leveridge and Shail, 2011; Strachan et al., 2014). The late faulting also separates the Traboe and (northern) Landewednack Hornblende Schists and the Crousa Downs Gabbro (Fig. 2), leading to divergent interpretation of their relationships (consanguineous and coeval? unrelated?). Based on new data in this paper, this issue is explored in the Discussion section.

3. Analytical methods

3.1. *Sample locations and descriptions*

The samples in this study were collected by D.H. Green in the early 1960s, and the zircon and baddeleyite analytical work presented here was mostly undertaken in the early 2000s. Detailed sample descriptions and exact sample sites (i.e., within a few metres accuracy) are no longer available. Instead, sample locations have been reconstructed in Google Earth™ from descriptions provided by D.H. Green 20 years ago to the first author, and are in supplementary Table 1 (with the Australian National University collection numbers used in this paper).

3.2. *Sample preparation*

Together with chips of reference zircons SL13 and Temora and the baddeleyite Phalaborwa, hand-picked zircons and baddeleyites were

Table 1
SHRIMP U/Pb zircon and baddelyite data.

		U	Th	Th/U	204Pb/206Pb			238 U/206Pb			207Pb/206Pb			age 206Pb/238 U		
spot	petrography	(ppm)	(ppm)					(unc)			(unc)			(Ma, corr)		
97-267 Landewednack hornblende schist (volcanosedimentary?)																
1.1	m,osc,p,fr	286	117	0.41	0.00068	±	0.00021	12.859	±	0.377	0.0639	±	0.0039	480.0	±	13.8
2.1	m,osc,eq	202	59	0.29	0.00019	±	0.00013	12.661	±	0.571	0.0618	±	0.0020	488.5	±	21.3
3.1	m,osc,p	308	139	0.45	0.00023	±	0.00012	13.740	±	0.668	0.0613	±	0.0018	451.7	±	21.3
4.1	e,osc,p	148	61	0.41	0.00059	±	0.00032	12.967	±	0.622	0.0626	±	0.0014	477.0	±	22.1
5.1	m,osc,p,fr	119	45	0.38	0.00039	±	0.00031	12.469	±	0.576	0.0715	±	0.0040	490.0	±	22.0
6.1	m,osc,eq,fr	156	55	0.35	0.00023	±	0.00019	12.369	±	0.533	0.0585	±	0.0016	501.6	±	20.9
7.1	e,osc,p,fr	149	45	0.30	0.00019	±	0.00016	12.811	±	0.595	0.0649	±	0.0013	481.2	±	21.6
8.1	e,osc,p,fr	193	80	0.41	0.00016	±	0.00012	13.177	±	0.519	0.0641	±	0.0024	468.7	±	17.9
9.1	m,p,osc	139	59	0.42	0.00042	±	0.00026	12.759	±	0.572	0.0630	±	0.0015	484.2	±	21.0
10.1	m,p,osc	174	85	0.49	0.00040	±	0.00022	13.134	±	0.703	0.0651	±	0.0019	469.7	±	24.3
11.1	m,osc,p	144	54	0.38	0.00025	±	0.00029	13.465	±	0.674	0.0683	±	0.0037	456.8	±	22.2
96–546 pelite layer - Landewednack hornblende schist																
1.1	c?osc,p,fr	516	659	1.28	0.00037	±	0.00008	10.340	±	0.251	0.0662	±	0.0009	590.2	±	13.7
1.2	r/rex?p,fr	1581	269	0.17	0.00030	±	0.00008	10.905	±	0.644	0.0614	±	0.0015	564.1	±	32.0
1.3	c?osc,p,fr	995	78	0.08	0.00023	±	0.00018	12.705	±	0.420	0.0620	±	0.0015	486.7	±	15.5
2.1	c + r?osc,p	552	272	0.49	0.00210	±	0.00034	11.304	±	0.309	0.0903	±	0.0018	526.5	±	13.9
2.2	c + r?osc,p	730	70	0.10	0.00062	±	0.00032	11.570	±	0.413	0.0683	±	0.0020	528.5	±	18.2
4.1	c,osc,p	616	508	0.82	0.00195	±	0.00017	9.675	±	0.243	0.0880	±	0.0014	612.7	±	14.7
4.2	r,osc/h,p	750	26	0.03	0.00352	±	0.00071	13.611	±	0.419	0.0955	±	0.0038	437.0	±	13.2
5.1	c,osc,p,fr	375	553	1.48	0.00649	±	0.00054	9.835	±	0.367	0.1638	±	0.0024	547.6	±	19.7
5.2	c + r?h,p,fr	965	104	0.11	0.01753	±	0.00181	9.940	±	0.280	0.2848	±	0.0082	449.9	±	13.7
6.1	c,osc,p	614	653	1.06	0.00085	±	0.00012	9.902	±	0.243	0.0735	±	0.0009	609.8	±	14.3
6.2	c + r?h,p	1240	233	0.19	0.00261	±	0.00050	11.615	±	0.357	0.0892	±	0.0047	513.2	±	15.5
7.1	c,osc,p	2002	255	0.13	0.00005	±	0.00002	12.067	±	0.283	0.0583	±	0.0005	513.8	±	11.6
7.2	r,h,p	1779	387	0.22	0.00239	±	0.00040	14.209	±	0.357	0.0938	±	0.0032	420.1	±	10.4
7.3	r,h,p	1277	105	0.08	0.00174	±	0.00035	15.358	±	0.421	0.0750	±	0.0018	398.8	±	10.7
8.1	m,osc,stubby	273	137	0.50	0.00257	±	0.00029	11.865	±	0.321	0.0950	±	0.0025	499.6	±	13.1
8.2	m,osc,stubby	680	64	0.09	0.00193	±	0.00053	11.825	±	0.766	0.0868	±	0.0035	505.9	±	31.7
9.1	m,h,stubby	575	195	0.34	0.00018	±	0.00006	12.277	±	0.297	0.0596	±	0.0007	504.5	±	11.8
10.1	c,osc,p	653	211	0.32	0.00125	±	0.00020	12.814	±	0.333	0.0837	±	0.0021	470.4	±	11.9
10.2	r,h,p	1054	68	0.06	0.00025	±	0.00005	13.197	±	0.575	0.0585	±	0.0010	471.2	±	19.8
10.3	r,h,p	695	146	0.21	0.00075	±	0.00019	12.788	±	0.740	0.0648	±	0.0014	482.1	±	27.0
11.1	c,h,stubby	1169	869	0.74	0.00010	±	0.00003	8.206	±	0.193	0.0661	±	0.0004	735.3	±	16.4
11.2	c + r?h,stubby	1098	151	0.14	0.00516	±	0.00100	13.192	±	0.439	0.1310	±	0.0097	430.2	±	14.9
analysis 3.1 aborted																
97-712 granodiorite intrusive sheet in Old Lizard Head Series																
1.1	m,osc,stubby	830	212	0.26	0.00012	±	0.00008	12.579	±	0.487	0.0584	±	0.0007	493.6	±	18.4
2.1	e,osc,stubby	1780	403	0.23	0.00005	±	0.00003	12.242	±	0.249	0.0575	±	0.0006	507.1	±	9.9
3.1	e,osc,p	843	252	0.30	0.00052	±	0.00010	12.941	±	0.434	0.0647	±	0.0014	476.7	±	15.5
4.1	e,osc,stubby	2505	548	0.22	0.00009	±	0.00003	13.599	±	1.290	0.0581	±	0.0005	458.0	±	42.1
5.1	e,h,stubby	1538	285	0.19	0.00003	±	0.00002	12.527	±	0.593	0.0573	±	0.0005	496.2	±	22.6
5.2	m,h,stubby	433	102	0.24	0.00007	±	0.00004	12.758	±	0.374	0.0573	±	0.0010	487.6	±	13.8
6.1	e,osc,stubby	1570	216	0.14	0.00033	±	0.00007	13.157	±	0.378	0.0613	±	0.0004	471.0	±	13.1
6.2	e,osc,stubby	883	161	0.18	0.00043	±	0.00009	13.054	±	0.845	0.0621	±	0.0007	474.1	±	29.7
6.3	m,osc,stubby	745	158	0.21	0.00006	±	0.00004	11.952	±	1.797	0.0583	±	0.0025	518.5	±	75.3
7.1	e,osc,stubby	1053	176	0.17	0.00005	±	0.00005	13.019	±	0.500	0.0577	±	0.0008	477.9	±	17.7
7.2	e,osc,stubby	2172	231	0.11	0.00012	±	0.00003	11.198	±	1.196	0.0589	±	0.0006	551.5	±	56.7
8.1	e,osc,stubby	1037	284	0.27	0.00003	±	0.00002	12.886	±	0.375	0.0571	±	0.0005	483.0	±	13.6
9.1	e/r?osc,stubby	3604	310	0.09	0.00075	±	0.00006	12.220	±	0.845	0.0675	±	0.0006	502.0	±	33.5
10.1	e,osc,stubby	3666	340	0.09	0.00015	±	0.00002	13.030	±	0.797	0.0585	±	0.0012	477.0	±	28.2

(*continued on next page*)

Table 1 (*continued*)

		U	Th	Th/U	204Pb/206Pb			238 U/206Pb			207Pb/206Pb			age 206Pb/238 U		
11.1	m,osc,stubby	919	256	0.28	0.00004	±	0.00003	12.597	±	0.552	0.0576	±	0.0006	493.4	±	20.8
12.1	m,osc,stubby	2325	808	0.35	0.00003	±	0.00003	12.773	±	0.749	0.0575	±	0.0004	486.9	±	27.6
97-719 granodiorite layer (intrusive sheet?) in Old Lizard Head Series																
1.1	m,osc/h,p	1946	340	0.17	0.00004	±	0.00002	12.229	±	0.272	0.0572	±	0.0005	507.9	±	10.9
1.2	m,osc/h,p	1353	244	0.18	0.00010	±	0.00003	12.751	±	0.541	0.0590	±	0.0015	486.8	±	19.9
2.1	m,osc,p	919	177	0.19	0.00006	±	0.00005	12.325	±	0.261	0.0578	±	0.0007	503.7	±	10.3
3.1	m,osc,p	742	192	0.26	0.00033	±	0.00007	12.929	±	1.371	0.0625	±	0.0029	478.3	±	49.1
3.2	e,osc,p	1192	358	0.30	0.00116	±	0.00019	12.335	±	0.465	0.0747	±	0.0015	493.2	±	17.9
4.1	m,osc/h,p	897	205	0.23	0.00003	±	0.00003	12.537	±	0.445	0.0576	±	0.0009	495.6	±	17.0
4.2	e,p,X	1414	281	0.20	0.00002	±	0.00001	13.028	±	0.314	0.0572	±	0.0006	477.9	±	11.1
5.1	m,osc,p	769	234	0.30	0.00009	±	0.00005	12.751	±	0.920	0.0555	±	0.0008	488.8	±	34.1
5.2	e,osc,p	1114	320	0.29	0.00007	±	0.00002	12.741	±	0.237	0.0578	±	0.0008	487.9	±	8.8
6.1	m,osc/h,p	562	109	0.19	0.00040	±	0.00012	12.155	±	0.387	0.0609	±	0.0008	508.6	±	15.6
7.1	m,osc/rex,stubby	981	381	0.39	0.00001	±	0.00001	11.789	±	0.262	0.0573	±	0.0008	526.0	±	11.3
8.1	e,osc/h,p	1312	477	0.36	0.00008	±	0.00003	12.335	±	0.404	0.0569	±	0.0007	503.8	±	15.9
9.1	m,osc,stubby	618	147	0.24	0.00105	±	0.00020	12.401	±	0.452	0.0723	±	0.0013	492.1	±	17.3
10.1	e,osc/h,p	1226	205	0.17	0.00007	±	0.00002	12.346	±	0.346	0.0581	±	0.0009	502.7	±	13.6
11.1	e,osc/h,p	1617	487	0.30	0.00011	±	0.00003	12.462	±	0.267	0.0570	±	0.0008	498.9	±	10.3
02–121 Man O'War gneiss																
1.1	e,osc,p	369	78	0.21	0.00028	±	0.00012	12.947	±	0.704	0.0610	±	0.0021	478.5	±	25.1
2.1	e,osc,p	666	270	0.40	0.00001	±	0.00000	11.892	±	0.425	0.0577	±	0.0011	521.4	±	18.0
2.2	e,osc,p	456	104	0.23	0.00012	±	0.00007	11.571	±	0.618	0.0610	±	0.0014	533.2	±	27.4
3.1	e,osc,p,fr	660	132	0.20	0.00042	±	0.00011	12.184	±	0.352	0.0635	±	0.0008	505.9	±	14.1
4.1	m,osc,p,fr	658	140	0.21	0.00007	±	0.00007	12.575	±	0.577	0.0579	±	0.0013	494.0	±	21.9
5.1	e,osc,p	693	191	0.28	<0.00001	±	0.00006	12.990	±	0.442	0.0586	±	0.0006	478.4	±	15.7
6.1	e,osc,p	981	226	0.23	<0.00001	±	0.00001	12.323	±	0.490	0.0575	±	0.0007	504.0	±	19.3
7.1	e,osc,p,fr	552	135	0.24	0.00013	±	0.00007	12.235	±	0.545	0.0577	±	0.0008	507.4	±	21.8
8.1	e,osc,p,fr	532	133	0.25	<0.00001	±	0.00005	13.265	±	0.493	0.0578	±	0.0007	469.3	±	16.9
9.1	e,osc,p	915	200	0.22	0.00016	±	0.00008	12.523	±	0.365	0.0599	±	0.0007	494.8	±	13.9
10.1	m,osc,p	816	213	0.26	0.00010	±	0.00003	12.176	±	0.513	0.0577	±	0.0006	509.7	±	20.7
10.2	e,rex,p	241	44	0.18	0.00034	±	0.00012	13.135	±	0.506	0.0653	±	0.0024	469.6	±	17.5
11.1	m,rex,p,fr	381	40	0.11	0.00135	±	0.00061	13.406	±	0.626	0.0740	±	0.0041	455.5	±	20.7
97-277 Traboe granulite																
1.1	m,osc,p	557	149	0.27	0.00030	±	0.00015	13.921	±	0.380	0.0576	±	0.0012	446.4	±	11.9
1.2	m,osc,p	615	189	0.31	0.00012	±	0.00007	14.638	±	0.956	0.0565	±	0.0010	424.6	±	27.1
2.1	m,osc,p,fr	925	149	0.16	0.00016	±	0.00004	12.114	±	0.359	0.0566	±	0.0016	509.8	±	14.7
3.1	m,osc,p,fr	626	92	0.15	0.00019	±	0.00006	13.471	±	0.354	0.0586	±	0.0011	461.3	±	11.8
4.1	m,osc,p,fr	1182	295	0.25	0.00004	±	0.00002	13.100	±	0.526	0.0568	±	0.0005	472.9	±	18.4
4.2	e,rex/hb,p,fr	122	11	0.09	0.00027	±	0.00014	13.919	±	0.459	0.0613	±	0.0015	446.1	±	14.3
5.1	m,osc,p	500	67	0.13	0.00006	±	0.00004	12.844	±	1.060	0.0554	±	0.0018	485.5	±	38.7
6.1	m,osc/nl,eq,fr	1426	286	0.20	0.00009	±	0.00005	12.583	±	0.433	0.0564	±	0.0006	494.6	±	16.4
7.1	m,osc,p	415	77	0.19	0.00004	±	0.00005	12.907	±	0.795	0.0570	±	0.0018	479.8	±	28.7
8.1	e,osc/rex,eq	276	46	0.17	0.00035	±	0.00012	15.578	±	0.659	0.0592	±	0.0009	401.1	±	16.5
9.1	e,osc,eq	200	65	0.33	0.00042	±	0.00017	12.687	±	0.424	0.0641	±	0.0041	486.2	±	15.9
10.1	m,osc,p,fr	344	59	0.17	0.00019	±	0.00011	12.975	±	0.817	0.0598	±	0.0017	478.3	±	29.1
11.1	m,osc,eq	452	109	0.24	0.00005	±	0.00007	13.172	±	0.656	0.0615	±	0.0015	470.4	±	22.6
96–532 Pyroxene granulite facies sheet in recrystallised peridotite																
1.1	m,osc,p	185	136	0.73	0.00029	±	0.00019	15.482	±	0.429	0.0578	±	0.0018	402.8	±	10.9
2.1	e,osc,p	214	143	0.67	0.00022	±	0.00014	16.210	±	0.458	0.0546	±	0.0016	383.8	±	10.6
3.1	m,osc,p	374	162	0.43	0.00006	±	0.00004	15.556	±	0.435	0.0556	±	0.0009	399.9	±	10.9
4.1	m,h,p	229	136	0.59	0.00014	±	0.00008	16.726	±	0.664	0.0555	±	0.0012	372.7	±	14.4

(*continued on next page*)

Table 1 (*continued*)

		U	Th	Th/U	204Pb/206Pb			238 U/206Pb			207Pb/206Pb			age 206Pb/238 U		
5.1	m,osc/h,eq	514	184	0.36	0.00002	±	0.00004	16.878	±	0.810	0.0568	±	0.0015	370.0	±	17.3
6.1	m,osc,fr	325	181	0.56	0.00003	±	0.00003	17.686	±	1.099	0.0551	±	0.0019	352.8	±	21.5
7.1	osc/sz,fr	181	124	0.69	<0.00001	±	0.00004	16.775	±	0.518	0.0565	±	0.0023	372.1	±	11.2
7.2	osc/sz,fr	148	87	0.59	0.00012	±	0.00016	16.553	±	0.607	0.0568	±	0.0016	377.1	±	13.5
7.3	osc/sz,fr	128	66	0.51	0.00006	±	0.00009	16.225	±	0.546	0.0556	±	0.0020	383.9	±	12.6
8.1	c,nl,p	1148	984	0.86	0.00006	±	0.00002	13.831	±	0.514	0.0564	±	0.0008	448.5	±	16.2
8.2	c,nl,p	939	787	0.84	0.00015	±	0.00005	12.918	±	0.291	0.0589	±	0.0005	444.4	±	10.4
9.1	c,nl,p	1674	1804	1.08	0.00002	±	0.00003	13.985	±	0.517	0.0575	±	0.0004	388.6	±	15.9
9.2	c,nl,p	1075	1003	0.93	<0.00001	±	0.00014	16.000	±	1.118	0.0544	±	0.0014	480.5	±	26.6
9.3	c,nl,p	1747	2232	1.28	0.00010	±	0.00002	12.769	±	0.283	0.0577	±	0.0007	485.3	±	10.4
9.4	c,nl,p	1632	2465	1.51	0.00016	±	0.00003	13.051	±	0.231	0.0574	±	0.0008	474.9	±	8.1
9.5	c,nl,p	1899	1602	0.84	0.00009	±	0.00002	15.238	±	0.199	0.0559	±	0.0003	408.2	±	5.2
96–558 Pyroxene granulite facies sheet in recrystallised peridotite																
1.1	e,h/sz,eq	20	10	0.52	<0.00001	±	0.00064	15.051	±	0.618	0.0636	±	0.0043	416.9	±	16.6
2.1	c,nl,eq	62	40	0.65	0.00032	±	0.00026	16.097	±	0.930	0.0614	±	0.0024	389.6	±	21.8
3.1	c,osc/rex,eq	22	12	0.56	0.00158	±	0.00077	14.403	±	0.837	0.0539	±	0.0051	430.0	±	24.7
4.1	e,h/sz,fr	34	30	0.87	<0.00001	±	0.00068	17.044	±	0.971	0.0574	±	0.0034	366.8	±	20.5
5.1	e,h/sz,eq	90	77	0.85	0.00023	±	0.00020	15.918	±	0.496	0.0562	±	0.0017	391.4	±	12.0
6.1	c?hd/rex,eq	818	281	0.34	0.00001	±	0.00002	15.926	±	0.868	0.0585	±	0.0013	392.3	±	20.8
7.1	c?osc/rex,eq	102	61	0.60	0.00004	±	0.00004	14.844	±	0.798	0.0569	±	0.0016	419.1	±	22.0
7.2	c?osc/rex,eq	114	68	0.60	0.00007	±	0.00014	16.490	±	0.772	0.0579	±	0.0019	379.0	±	17.3
8.1	nl,fr	130	49	0.37	0.00015	±	0.00013	15.695	±	0.633	0.0608	±	0.0027	399.0	±	15.6
9.1	e,osc/nl,p,fr	287	52	0.18	0.00015	±	0.00010	16.003	±	0.622	0.0549	±	0.0010	388.7	±	14.8
10.1	c?osc/rex,eq	109	73	0.67	0.00015	±	0.00011	15.655	±	0.808	0.0584	±	0.0029	398.8	±	20.1
11.1	c?osc,p,fr	1344	700	0.52	0.00009	±	0.00003	15.739	±	0.449	0.0558	±	0.0004	395.5	±	11.0
GA2567 Crousa Downs Gabbro																
baddelyites																
5.1		47	1	0.02	0.02022	±	0.00121	9.390	±	0.378	0.2868	±	0.0070	473.7	±	19.3
5.2		24	0.2	0.01	0.01360	±	0.00277	11.671	±	0.468	0.2146	±	0.0192	430.5	±	20.8
A.1		35	0.2	0.01	<0.00001			14.940	±	0.746	0.0739	±	0.0123	417.6	±	30.6
A.2		44	1.1	0.03	0.01300	±	0.01200	13.200	±	0.520	0.2050	±	0.0170	372.8	±	24.0
6.1		26	4	0.15	0.00174	±	0.00074	15.215	±	0.685	0.0675	±	0.0023	406.2	±	17.8
6.2		29	3	0.12	0.00387	±	0.00099	13.793	±	0.653	0.1034	±	0.0038	427.1	±	19.7
B.1		26	1	0.03	<0.00001			15.600	±	0.637	0.0094	±	0.0220	396.5	±	32.1
B.2		38	11	0.28	0.00940	±	0.01300	13.160	±	0.420	0.0111	±	0.3260	428.6	±	20.9
zircons																
1.1	e,h,fr	166	214	1.29	0.00009	±	0.00010	16.046	±	0.438	0.0557	±	0.0010	391.4	±	10.4
1.2	m,h,fr	169	214	1.26	0.00002	±	0.00002	16.674	±	0.484	0.0550	±	0.0020	377.4	±	10.7
1.3	e,h,fr	311	359	1.16	<0.00001	±	0.00005	16.569	±	2.361	0.0541	±	0.0029	380.1	±	52.8
2.1	h,eq	106	113	1.06	0.00008	±	0.00007	15.348	±	0.437	0.0542	±	0.0013	409.3	±	11.3
3.1	h,eq/fr	777	1640	2.11	0.00003	±	0.00001	15.763	±	0.507	0.0541	±	0.0008	398.9	±	12.5
4.1!	h,eq	118	35	0.30	0.00012	±	0.00007	5.748	±	0.150	0.0749	±	0.0007	1015.1	±	24.5

* all zircon analyses; spot = grain and site I.D., all analytical errors given at the 1 sigma level grain type and analytical site; e = grain end or edge, m = grain middle/centre; eq = equant, p = prism, fr = grain fragment, spot CL domain characteristics; osc = oscillatory zoning; sz = sector zoning; rex = recrystallisation;
c = structural core, h = homogeneous, hb = homogeneous and bright; nl = non-luminescent.
! possible mineral separation contaminant grain (very small yield of zircons).
$^{204}Pb/^{206}Pb$ <0.00001 - when counting very small numbers of ^{204}Pb ions, background counts can be randomly higher, giving a negative $^{204}Pb/^{206}Pb$ ratio. In such cases the ratio has been adjusted, indicated as <0.00001 in the table.
$^{238}U/^{206}Pb$ and $^{207}Pb/^{206}Pb$ are uncorrected for common Pb.
$^{206}Pb/^{238}U$ age (Ma) corrected for common Pb by the '207' method (Compston et al., 1984).

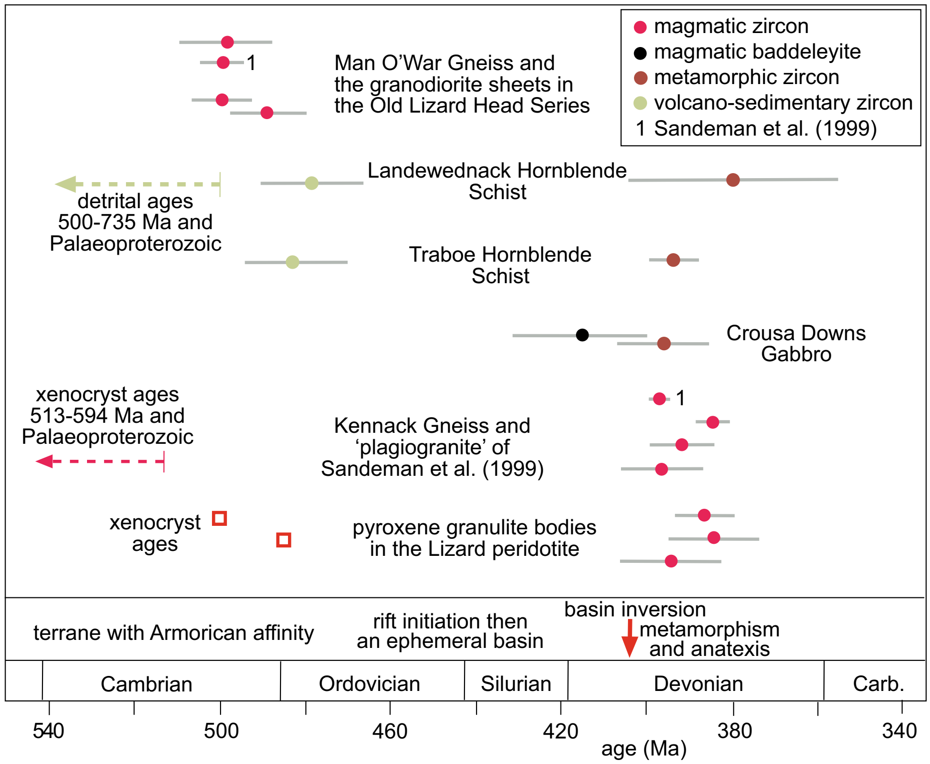

Fig. 4. Summary of U-Pb zircon and baddeleyite ages from the Lizard Complex.

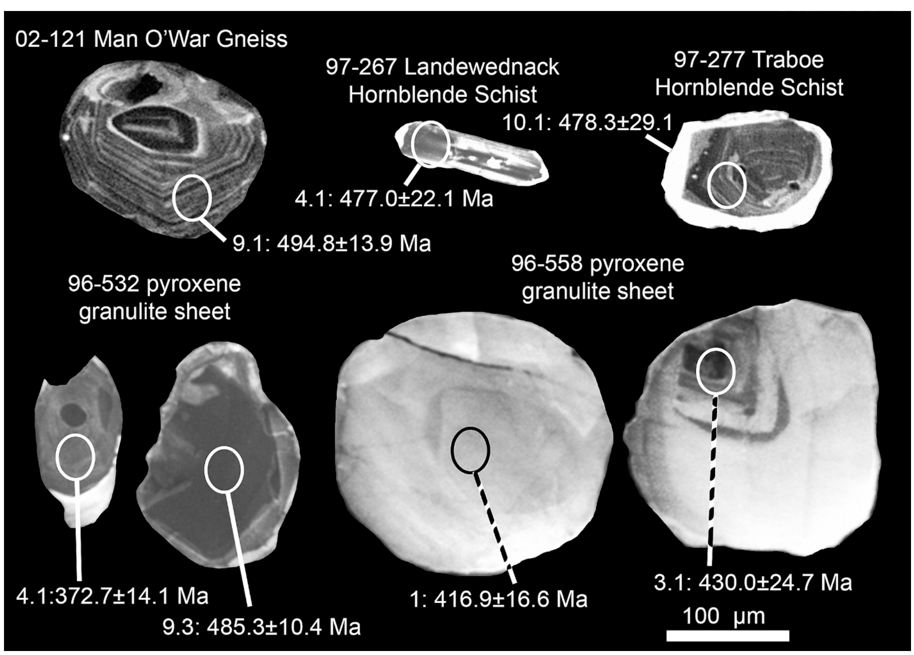

Fig. 5. Representative cathodoluminescence images of samples 02-121, 97-267, 97-277, 96-532 and 96-558 (see text for explanations).

cast into 1″ epoxy resin discs and then cut and polished to present sections of grains for analysis. Assessment of the grains and the choice of sites for analysis was based on transmitted/reflected light microscopy and cathodoluminescence imaging (CL). Additionally, by SEM, Zr and Si mapping and BSE imaging was undertaken on the two small (ca. 50 µm) baddeleyite grains recovered from the Crousa Downs Gabbro sample GA2567.

3.3. *U-Pb zircon and baddeleyite SHRIMP operating conditions and data reduction*

Zircon and baddeleyite U-Pb isotopic data (Table 1) were obtained from the Australian National University (ANU) SHRIMP II instrument. Typically a ca. 30 µm diameter spot was used with a mass-filtered O^{2-} primary ion beam of 3 to 4 nA. A secondary beam with a mass resolution of 5500 to 6000 (measured at 1% peak height) was used for analysis. Under these conditions all significant near isobaric interferences close to the Pb^+ peaks are avoided. Details of the analytical procedure are presented by Stern (1998) and Williams (1998).

SL13 was used as a U abundance standard (U = 238 ppm). Due to differential yield of metal and oxide cation species between elements during sputtering by the focussed O^{2-} primary ion beam, inter-element ratios are calibrated with a reference material with the same matrix (mineral species), and whose isotopic ratios are known by isotope dilution thermal ionisation mass spectrometry (IDTIMS). The calibration method is explained by Stern (1998) and Williams (1998). Thus $^{206}Pb/^{238}U$ ratios have an error component (typically 1.5 to 2.0%) from calibration of the measurements using the reference zircons and baddeleyites, which is added in quadrature to the $^{206}Pb/^{238}U$ internal analytical uncertainty of each analysis. Temora-1 with $^{238}U/^{206}Pb$ age of 417 Ma (Black et al., 2003) was used to calibrate the U-Pb data of the unknown zircons. Phalaborwa baddeleyite was used to calibrate the U-Pb data of the Crousa Downs Gabbro baddeleyites. Phalaborwa baddeleyite grains which have been chemically abraded show a concordant U-Pb age of 2060 Ma (Heaman, 2009). However, untreated grains such as used as reference materials for in situ analysis display variable degrees of modern radiogenic Pb loss, giving rise to a spread of $^{238}U/^{206}Pb$ ages of ≤2060 Ma, at a constant $^{207}Pb/^{206}Pb$ age of 2060 Ma (White et al., 2020). Thus in the case of erecting a U-Pb calibration for the Crousa Downs Gabbro baddeleyites, reference Phalaborwa analyses with (i) the youngest apparent $^{238}U/^{206}Pb$ ages and (ii) $^{90}Zr_2^{16}O^+$ count rates markedly different from the Crousa Downs Gabbro baddeleyites were not used.

The decay constants and present-day $^{238}U/^{235}U$ value given by Steiger and Jäger (1977) were used to calculate dates, which are derived from $^{206}Pb/^{238}U$ ratios, following correction for common Pb by the ^{207}Pb method (Compston et al., 1984) and use of the Cumming and Richards (1975) model Pb composition for the likely age of the zircons. Dates calculated in this paper are weighted mean $^{206}Pb/^{238}U$ dates (analyses inverse-variance weighted, 95% confidence), based on grouping of sites interpreted from CL images to belong to one generation of zircon. The dates were calculated using the program Isoplot/Ex of Ludwig (1998). Results are summarised in Fig. 4 where they are

Table 2
Summary Lu-Hf data for Lizard Complex samples.

Analysis	$^{176}Lu/^{177}Hf$		1SE	Measured $^{176}Hf/^{177}Hf$		1SE	Present day eHf(0)[A]		1SE	Initial eHf(t)
96–532 pyroxene granulite sheet in peridotite										
96–532.1	0.000729	±	0.000003	0.282505	±	0.000010	−9.9	±	0.37	−1.5
96–532.2	0.000413	±	0.000002	0.282625	±	0.000036	−5.7	±	1.26	2.8
96–532.3	0.000806	±	0.000049	0.282626	±	0.000017	−5.6	±	0.61	2.8
96–532.4	0.000041	±	0.000001	0.282629	±	0.000023	−5.5	±	0.81	3.1
96–532.5	0.000136	±	0.000001	0.282629	±	0.000011	−5.5	±	0.40	3.0
96–532.6	0.000086	±	0.000001	0.282685	±	0.000014	−3.5	±	0.51	5.0
96–532.7	0.001537	±	0.000019	0.282688	±	0.000013	−3.4	±	0.47	4.8
96–532.7B	0.000349	±	0.000000	0.282631	±	0.000018	−5.5	±	0.65	3.1
96–532.8	0.001822	±	0.000050	0.282719	±	0.000087	−2.3	±	3.07	7.9
96–532.A	0.000678	±	0.000001	0.282563	±	0.000015	−7.8	±	0.52	0.6
96–532.B	0.000073	±	0.000000	0.282558	±	0.000014	−8.0	±	0.48	0.6
96–532.C	0.000748	±	0.000011	0.282673	±	0.000016	−4.0	±	0.55	4.5
96–532.D	0.000060	±	0.000001	0.282633	±	0.000009	−5.4	±	0.33	3.2
96–532.E	0.000024	±	0.000000	0.282630	±	0.000011	−5.5	±	0.40	3.1
96–558 pyroxene granulite sheet in peridotite										
96–558.1	0.000498	±	0.000005	0.282454	±	0.000011	−11.7	±	0.41	−3.0
96–558.2	0.000335	±	0.000014	0.282445	±	0.000011	−12.0	±	0.40	−3.3
96–558.2B	0.000217	±	0.000002	0.282441	±	0.000017	−12.1	±	0.60	−3.4
96–558.5	0.000344	±	0.000003	0.282446	±	0.000014	−12.0	±	0.50	−3.3
96–558.7	0.000691	±	0.000017	0.282454	±	0.000015	−11.7	±	0.53	−3.1
96–558.9	0.000876	±	0.000010	0.282586	±	0.000014	−7.0	±	0.49	1.6
96–558.10	0.000119	±	0.000008	0.282406	±	0.000014	−13.4	±	0.48	−4.6
96–558.11	0.000363	±	0.000024	0.282318	±	0.000013	−16.5	±	0.47	−7.8
96–558.A	0.000340	±	0.000011	0.282451	±	0.000016	−11.8	±	0.57	−3.1
96–558.B	0.000062	±	0.000002	0.282447	±	0.000014	−12.0	±	0.51	−3.2
96–558.C	0.000435	±	0.000010	0.282405	±	0.000016	−13.4	±	0.55	−4.7
96–558.D	0.000065	±	0.000002	0.282467	±	0.000011	−11.3	±	0.39	−2.5
96–558.E	0.000062	±	0.000000	0.282434	±	0.000013	−12.4	±	0.46	−3.6
96–558.F	0.000209	±	0.000001	0.282432	±	0.000017	−12.5	±	0.62	−3.7
96–558.G	0.000072	±	0.000001	0.282401	±	0.000012	−13.6	±	0.43	−4.8
GA2567 Crousa Downs Gabbro										
GA 2567.C	0.002518	±	0.000031	0.282918	±	0.000015	4.7	±	0.52	13.3
GA 2567.F	0.003625	±	0.000016	0.282989	±	0.000016	7.2	±	0.58	15.5
02–121 Man O'War Gneiss										
1667.1	0.001065	±	0.000005	0.282746	±	0.000010	−1.4	±	0.36	9.4
1667.2	0.001118	±	0.000026	0.282742	±	0.000011	−1.5	±	0.38	9.2
1667.3	0.001190	±	0.000017	0.282742	±	0.000011	−1.5	±	0.39	9.2
1667.4	0.000854	±	0.000003	0.282717	±	0.000011	−2.4	±	0.40	8.4
1667.5	0.001096	±	0.000014	0.282756	±	0.000010	−1.0	±	0.35	9.7
1667.6	0.001350	±	0.000013	0.282743	±	0.000012	−1.5	±	0.41	9.2
1667.7	0.001249	±	0.000008	0.282724	±	0.000011	−2.1	±	0.39	8.5
1667.8	0.001221	±	0.000033	0.282739	±	0.000019	−1.6	±	0.68	9.1
1667.9	0.000584	±	0.000005	0.282727	±	0.000013	−2.0	±	0.44	8.9
1667.1	0.001106	±	0.000007	0.282729	±	0.000008	−2.0	±	0.30	8.7
1667.B	0.001273	±	0.000017	0.282721	±	0.000008	−2.3	±	0.29	8.4
1667.D	0.001468	±	0.000025	0.282714	±	0.000010	−2.5	±	0.36	8.1

integrated with previous published age determinations, representative zircon images are shown in Fig. 5 and all data are presented graphically in Figs. 8-10 and 12 as $^{207}Pb/^{206}Pb$ – $^{238}U/^{206}Pb$ Tera-Wasserburg plots (uncorrected for common Pb) with histograms of the ^{207}Pb-corrected $^{238}U/^{206}Pb$ dates.

3.4. LA-MC-ICPMS Lu-Hf isotopic data

Zircon Lu-Hf isotopic compositions were determined from the same domains as the U-Pb geochronology, as determined by CL imagery. Most of these were positioned directly over the previous SHRIMP U-Pb analysis 1–2 µm-deep craters, with a minority of other analyses undertaken on other domains with relict oscillatory zoning displayed in CL images. Data were acquired during a single analytical session (24–25 November 2021) using the RSES ThermoFinnigan Neptune multi-collector (9 Faraday cups with 10^{11} Ω resistors) ICPMS coupled to a Lambda Physik ArF, 193 nm excimer laser system with a 'HelEx' sample cell, following methods described by Hiess et al. (2009) and using a 37 µm diameter spot. Analysis of a gas blank and a suite of 5 reference zircons with a range of $^{176}Hf/^{177}Hf$ and $^{176}Lu/^{177}Hf$ ratios (Mud Tank, Plesovice, QGNG, Temora-2 and FC1) were performed systematically after every 10–12 sample spot analyses throughout the session. Time slice data reduction using in-house developed software was used to monitor potential downhole variations in isotopic compositions resulting from drilling through different age zones. Mass bias corrections were made for Hf and for Lu and Yb prior to interference subtraction (Hiess et al., 2009).

The details of the analytical method and instrumental set-up are provided in the Supplementary Data. The $^{176}Hf/^{177}Hf$ isotopic compositions determined for the reference zircons are in all cases within uncertainty (<0.5 epsilon units) of accepted literature solution values.

Initial $^{176}Hf/^{177}Hf$ ratios for each spot were calculated using SHRIMP measured U-Pb ages, present day CHUR compositions of $^{176}Hf/^{177}Hf = 0.282785 \pm 11$, $^{176}Lu/^{177}Hf = 0.0336 \pm 1$ (Bouvier et al., 2008), and a λ^{176}Lu decay constant of $1.867 \pm 8 \times 10^{-11} y^{-1}$ (Scherer et al., 2001; Söderlund et al., 2004). Results are summarised in Table 2 and graphically as a zircon age versus initial εHf plot (Fig. 6). Complete Lu-Hf isotopic data for the sample zircons and for the reference zircons including $^{174}Hf/^{177}Hf$ and $^{178}Hf/^{177}Hf$ isotopic compositions are given in Supplementary Data Tables 1 and 2.

3.5. Zircon Rare Earth Element chemistry method

Zircons equilibrated in garnet-absent igneous and metamorphic systems typically show 1000 to 10,000 times enrichment in the heaviest

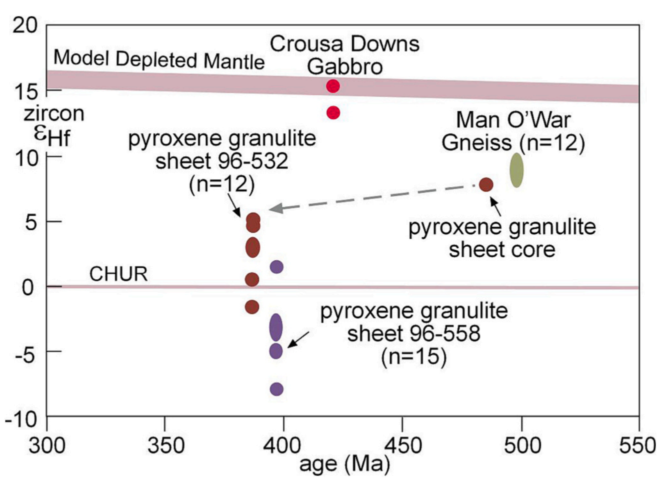

Fig. 6. Initial ε_{Hf} versus age of zircon (T) plot (typical ε_{Hf} uncertainty is ±0.5 epsilon unit).

Table 3
Zircon REE analyses.

Analysis	Site	Age (Ma)	P	Y	Th	U	Th/U	La	Ce	Pr	Nd	Sm	Eu	Gd	Tb	Dy	Ho	Er	Tm	Yb	Lu
02–121 Man O'War Gneiss																					
5	e,osc,p	478.4	294	867	176	656	0.27	0.13	23.60	0.568		15.70	16.16	66.2	124.1	254.3	479.1	915.1	1578		4044
7	e,osc,p,fr	507.4	324	766	119	501	0.24	0.07	18.29	0.615		13.75	15.02	57.5	113.9	229.3	426.6	805.3	1398		3640
8	e,osc,p,fr	469.3	242	616	116	584	0.20	0.05	13.09	0.791		18.10	18.43	65.8	107.7	200.3	352.9	634.7	1077		2749
9	e,osc,p	494.8	262	613	186	763	0.24	0.26	18.03	0.499		14.27	12.12	49.9	91.40	186.8	345.0	641.1	1095		2794
96–532 pyroxene granulite quartzfeldspathic sheet cutting recrystallised peridotite																					
4	m,h,p	372.7	164	167	213	274	0.78	bdl	5.63	0.769		20.80	10.42	61.0	74.95	97.3	110.7	123.3	137.6		153.8
5	m,osc/h,eq	370.0	184	149	153	445	0.34	0.06	3.13	0.077	1.07	1.21	0.43	5.5	1.51	15.9	5.10	21.4	4.34	39.3	6.56
8 core/comp**	c + r?,nl,p	≥448.5	386	540	224	345	0.65	0.07	3.40	0.122	1.43	2.38	0.31	15.5	4.58	54.7	18.09	82.4	16.88	149.8	23.10
8 rim	r,nl,p		176	107	136	221	0.61	bdl	1.76	0.034	0.52	1.02	0.24	4.6	1.24	12.9	3.79	14.7	2.71	23.81	3.90
9a	c,nl,p	485.0	1336	3747	2639	1915	1.38	1.19	30.81	0.684	7.28	11.75	1.45	79.8	26.41	347.2	123.3	555.3	114.1	1021.3	161.0
9b	c,nl,p	485.0	1194	5049	2657	1838	1.45	0.19	30.78	0.614	9.79	18.48	1.78	117.1	37.91	487.4	171.1	747.8	149.8	1308	203.8

grain morphology: eq = equant, p = prismatic, fr = grain fragment, e = grain end, m = grain middle, r = overgrowth, c = core.
CL imagery: osc = oscillatory zoned, h = homogeneous, nl = non-luminescent.
** start of analysis in grain centre at surface of the mount; * end of analysis on grain margin, at bottom of grain in the mount age is SHRIMP U-Pb age.

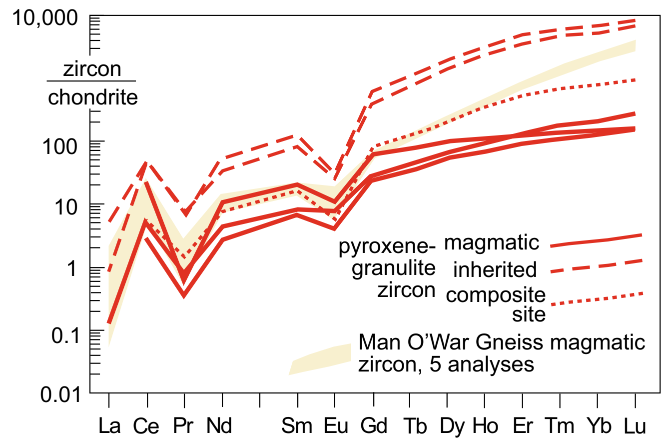

Fig. 7. Chondrite-normalised zircon rare earth element plot for zircons in pyroxene granite sheet 96–532 and Man O'War Gneiss sample 02–121.

REE relative to chondrite abundances. Conversely, zircons equilibrated with garnet typically show only 10 to 100 times enrichment, due to the strong affinity of the heavy REE for garnet (e.g., Rubatto et al., 2001). Thus zircon REE geochemistry is a powerful tool for understanding the phases zircons equilibrated with during their growth.

In situ measurement of zircon trace element abundances were obtained at RSES, ANU, using a Lambda Physik LPX 1201 UV ArF excimer laser coupled to an Aligent 7500 inductively coupled plasma mass spectrometer (LA-ICP-MS). The zircons in epoxy grain mounts were placed in an Ar-He flushed sample cell (Eggins et al., 1998), with the laser operated at constant voltage, 21–23 kV at 5 Hz, with a spot diameter of 29 to 50 μm. Ablated material was carried by the He-Ar gas via a custom-made flow homogeniser to the ICP-MS. Data were acquired for ca. 20 s with the laser turned off (for backgrounds) and c. 40 s with the laser on. This acquisition mode gives approximately 120 mass scans with a penetration depth of 20 μm. Each block of four unknowns was bracketed by analyses of glass standard NIST610. Raw count rates were converted into concentrations offline using an Excel™ spreadsheet (written by S. Eggins and C. Allen, ANU). Corrections for mass bias drift in unknowns were made using the bracketing NIST610 glass analyses (Norman et al., 1996). Trace element abundances are normalised using Zr_2O of 64 wt% in the zircons (appropriate for zircons with a few percent hafnon solid solution). Sites for laser ablation analyses were also chosen using the CL images as a guide and many were started over ca. 1 μm deep SHRIMP U/Pb dating analytical sites. Results are presented in Table 3 and as a chondrite-normalised REE plot (Fig. 7).

4. Results

4.1. Man-of-War Gneiss, sample 02-121

The Man-of-War Gneiss sample 02–121 with a weak tectonic foliation gave a large yield of zircons of prismatic habit, typically 100–150 μm long and displaying oscillatory zoning. The grains appear devoid of metamorphic overgrowth or inherited cores, and are interpreted as a simple magmatic population. Thirteen SHRIMP U-Th-Pb analyses were undertaken on 11 grains (Table 1; Figs. 5 and 8A). Most analyses have U abundance between 300 and 1000 ppm and Th/U ratios between 0.2 and 0.4, with close to concordant U-Pb ages. All analyses yield a weighted mean $^{238}U/^{206}Pb$ age of 493 ± 12 Ma (MSWD = 1.3). Excluding analyses 10.2 and 11.1 which have the highest measured $^{207}Pb/^{206}Pb$ and the youngest apparent $^{238}U/^{206}Pb$ ages (indicative of a higher common Pb content combined with some loss of radiogenic Pb), yields a weighted mean $^{238}U/^{206}Pb$ age of 498 ± 11 Ma (MSWD = 0.94), which is interpreted as the time of magmatic crystallisation of the Man-of-War Gneiss and consequently the maximum age of the observed ductile deformation within the sample. This agrees with the previously reported IDTIMS zircon U-Pb age of 499^{+8}_{-3} Ma reported by Sandeman et al. (1997).

Twelve Lu-Hf isotopic analyses were undertaken on the zircons, 10 of which were over previous SHRIMP U-Th-Pb analysis sites and 2 on randomly chosen other grains (Table 2). They yield a close range in εHf_{498} values of +8.1 to +9.7 (Table 1; Fig. 6) with model depleted mantle intercepts at ca. 700 Ma, indicative of involvement of older continental crust in the genesis of the Man-of-War Gneiss igneous protolith. LA-ICP-MS REE analyses were undertaken on 5 Man-of-War Gneiss zircons (Table 3). The chondrite normalised patterns (Fig. 7) indicate strong enrichment in the heavy REE (>8000 chondrite for Lu) with distinct negative Eu anomalies. As such, they display patterns typical of magmatic zircons in granitoids.

4.2. Granodiorite sheet intruded into the Old Lizard Head Series, sample 97-712

The Old Lizard Head Series at the Lizard Headland (Fig. 2) contains granodioritic bodies, some of which are discordant to compositional layering in the host rocks. Therefore they provide the minimum depositional age for the Old Lizard Head Series. Sample 97-712 of discordant granodiorite yielded abundant zircons which are prismatic in habit and display variably-recrystallised oscillatory zoning. Sixteen SHRIMP U-Th-Pb analyses were undertaken on 12 zircons (Table 1, Fig. 8B). The analyses indicate high U content (>400 ppm) and moderate Th/U (mostly 0.2 to 0.4). Apart from 4 analyses with higher measured $^{207}Pb/^{206}Pb$ between 0.06 and 0.07, all other analyses have concordant U-Pb ages (Fig. 8B). All analyses yield a weighted mean $^{238}U/^{206}Pb$ age of 488.4 ± 9.0 Ma (MSWD = 0.61), which is interpreted as the time of magmatic crystallisation of the granodioritic sheet. This provides the *minimum* depositional age for the Old Lizard Head Series.

4.3. Granodiorite concordant layer in the Old Lizard Head Series, sample 97-719

This foliated granodioritic concordant layer in the Old Lizard Head Series is probably a more strongly deformed version of the discordant granodioritic sheet 97-712 reported above. Fifteen SHRIMP U-Th-Pb analyses were undertaken on 11 grains (Table 1). The analyses indicate high U content (>500 ppm) and moderate Th/U (0.2 to 0.4). Apart from two analyses with higher measured $^{207}Pb/^{206}Pb$ between 0.07 and 0.08, all other analyses have close to concordant U-Pb ages (Fig. 8C). All analyses yield a weighted mean $^{238}U/^{206}Pb$ age of 498.9 ± 6.8 Ma (MSWD = 0.95), which is interpreted as the time of magmatic crystallisation of the granodioritic layer. This means that heterogeneous ductile deformation in the Old Lizard Head Series occurred at ≤500–490 Ma.

4.4. Pelitic layer in the Landewednack Hornblende Schists, sample 96–546

The Landewednack Hornblende Schists are interpreted to have protoliths of predominantly mafic lavas, tuffs with some dolerite dykes (Floyd et al., 1993; Jones, 1997), but contain rare pelitic schist layers. Previous zircon geochronology on a typical hornblende schist (sample 96/543) gave a small yield of low Th/U zircons with a weighted mean $^{238}U/^{206}Pb$ age of 379 ± 25 Ma, interpreted as giving the time of metamorphism (Nutman et al., 2001). Sample 97-546 of a pelitic schist layer from the same locality (Pen Olver; Fig. 2) gave a small yield of predominantly prismatic to somewhat rounded zircons. Twenty-two SHRIMP U-Th-Pb analyses were undertaken on 11 grains (Table 1; Fig. 9). The large number of multiple analyses on individual grains was in order to establish the most robust ages on cores with relict oscillatory zoning and to establish the age of metamorphic overgrowths. The data display variable incorporation of common Pb within the analytical sites, with almost half of the data having measured $^{207}Pb/^{206}Pb$ > 0.08, and

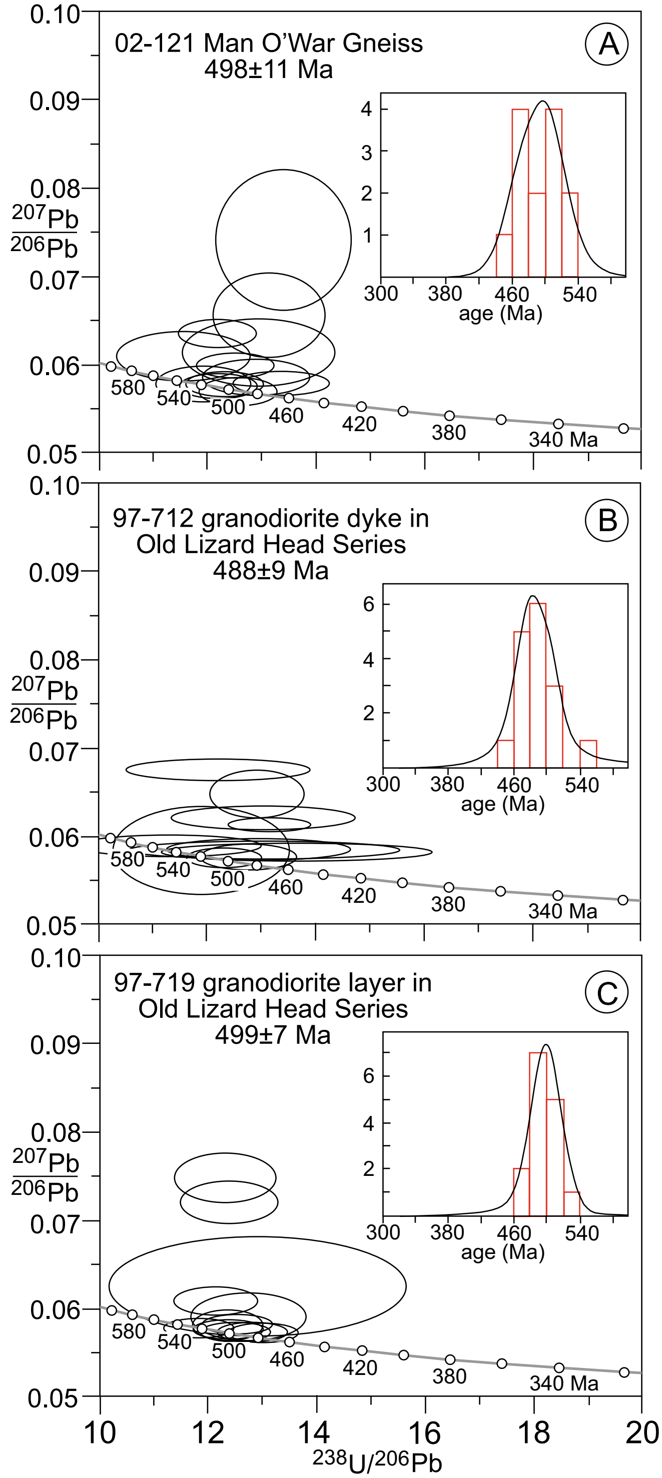

Fig. 8. $^{207}Pb/^{206}Pb$ versus $^{238}U/^{206}Pb$ Tera-Wasserburg plots (not corrected for common Pb) for samples 02-121, 97-712 and 97-719. The inserts in each Tera-Wasserburg plot are cumulate frequency distributions and histograms of the $^{206}Pb/^{238}U$ ages corrected for common Pb.

therefore show strongly discordant U-Pb ages (Fig. 9). Appraisal of the data is based on the less discordant analyses which have a smaller amount of common Pb in the targeted sites. Analyses of the cores with relict oscillatory zoning and with moderate to high Th/U (1.2 to 0.3) show a scatter of ages from ca. 490 Ma up to 735 Ma. These grains are interpreted to be detrital in origin, and indicate Cambrian and older (Neoproterozoic) rocks in the source region. Analyses of <500 Ma overgrowths are lower Th/U and have two ages; ca. 475 Ma (grain 10) and ca. 400 Ma (grain 7). Combining the metamorphic age rim determinations from this sample 96–546 with the low U, low Th/U metamorphic grains in hornblende schist sample 96–543 from the same locality (Nutman et al., 2001), yields a spread in $^{238}U/^{206}Pb$ ages beyond that expected from analytical uncertainty. These ages appear to be bimodal and mixture modelling of the data extracts two populations of separate thermal events at 407 ± 14 (Lower Devonian rifting?) and 361 ± 22 Ma (early Variscan convergence?).

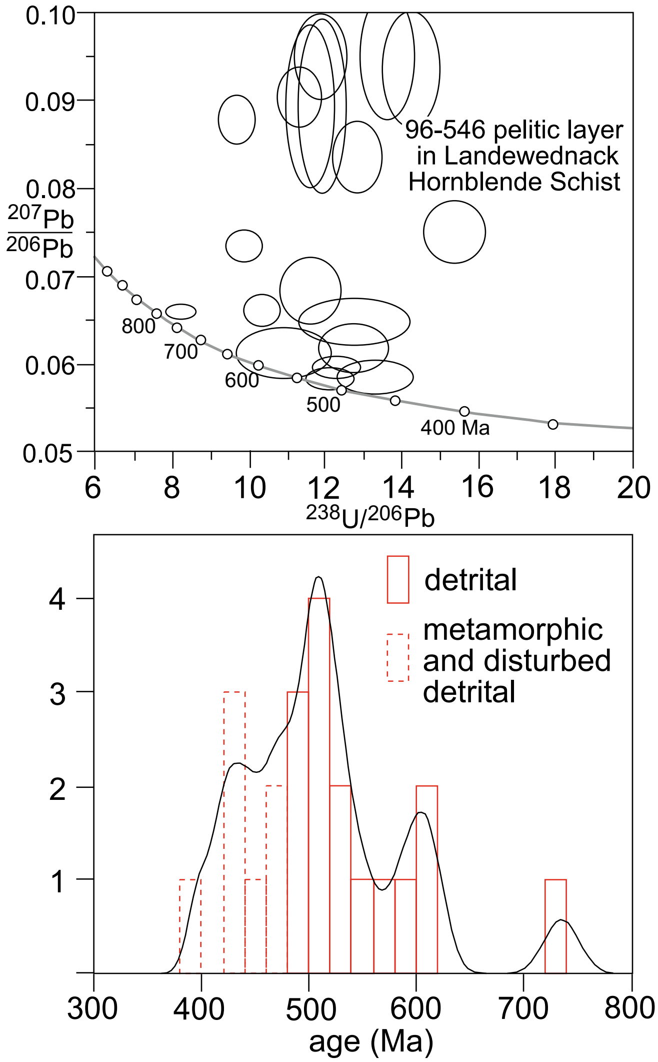

Fig. 9. For sample 96–719 (A) $^{207}Pb/^{206}Pb$ versus $^{238}U/^{206}Pb$ Tera-Wasserburg plot (not corrected for common Pb) and (B) the cumulate frequency distribution and histogram of the $^{206}Pb/^{238}U$ ages corrected for common Pb.

4.5. *Landewednack Hornblende Schist, sample 97-267*

Landewednack Hornblende Schist sample 97-267 from Pencra Head (Fig. 2) in the northwest of the Lizard Complex is a blue-green hornblende amphibolite with small zircons observed in thin section. The sample gave a small yield of prismatic to slightly rounded zircons with a maximum length of ca. 100 μm, but typically only ca. 50 μm. Given the small size and prismatic habit of the zircons they are likely to be volcanogenic in origin. The interior of the grains show broad to oscillatory zoning, with the grain exteriors are commonly marked by partial recrystallisation rims only a few micrometres thick that are bright in CL imagery (Fig. 5). Eleven SHRIMP U-Th-Pb analyses were undertaken on 11 grains (Table 1). The sites have moderate U content of between 140 and 310 ppm, with Th/U ratios between 0.29 and 0.49. Uncorrected for common Pb, all analyses show slightly discordant U-Pb ages (Fig. 10A). After correction for common Pb, all analyses have indistinguishable $^{238}U/^{206}Pb$ ages, with a weighted mean of 478.0 ± 12.0 Ma (MSWD = 0.48). This is interpreted as the age volcanism for the protolith of this sample.

4.6. *Traboe Hornblende Schist, sample 97-277*

Traboe Hornblende Schist sample 97-277 is from near Traboe Cross, the inland type locality for the lithology. It is a fine-grained green-brown hornblende + plagioclase amphibolite with a sub-vertical foliation. The sample gave a small yield of equant to stubby prismatic zircons 150 μm long. In CL images the grains display variably recrystallised oscillatory-zoned zircon, with narrow recrystallisation fringes which appear bright in CL images (Fig. 5). Thirteen SHRIMP U-Th-Pb analyses were undertaken on 11 zircons (Table 1). The analysed sites have moderate to high U content (200 to 1400 ppm) with moderate Th/U (mostly 0.15 to 0.33). All analyses have close to concordant U-Pb ages (Fig. 10B), but show a dispersion in $^{238}U/^{206}Pb$ beyond that expected from analytical error alone. Based on a model of some radiogenic Pb loss, rejecting 2 of the 13 analyses (including site #4.2 showing recrystallisation in CL imagery) yields a $^{238}U/^{206}Pb$ weighted mean age of 482.0 ± 12.0 Ma (MSWD = 0.99) for the remaining analyses. This is interpreted as giving the age of an igneous component (volcano-sedimentary?) in the sample.

4.7. *Crousa Downs Gabbro, sample GA2567*

The mineral separation of the Cousa Downs Gabbro sample GA2567 yielded 2 small (<50 μm) baddeleyite grains and 4 somewhat larger (up to 100 μm long) zircon grains. In CL imagery, both baddeleyite grains display oscillatory and sector zoning (Fig. 11). The smaller of the baddeleyite grains (#2) has an angular anhedral habit, and BSE imaging, silica and zirconium abundance mapping by EDS (energy dispersive spectrometry) demonstrate that this grain is unaltered (Fig. 11). On the other hand, the imagery of baddeleyite grain #1 shows partial recrystallisation to zircon around its margins (silicon detected and reduced zirconium), and it is cracked with alteration (Fig. 11). The zircon grains range from equant to angular anhedral in habit and in CL images are largely featureless and are devoid of oscillatory zoning. Based on their textures and evidence of partial recrystallisation of baddeleyite to zircon, the zircons are likely to be of post magmatic origin.

In the first analytical session in 2002, 2 analyses each were made on the 2 baddeleyite grains, and this was repeated in a 2022 analytical session with an extra 2 analyses each on the grains. In the first session, analysis 1.1 demonstrated a lower $^{90}Zr_2^{16}O^+$ count rate compared with the other analyses and also a higher apparent $^{238}U/^{206}Pb$ age (474 Ma). This suggests it might contain a significant mix of zircon with baddeleyite, which then with a different matrix effect could cause inaccuracy in the U-Pb calibration. Therefore it has been excluded from age assessment. The remaining analyses display a range in radiogenic versus common Pb as shown by their variable $^{207}Pb/^{206}Pb$ and hence dispersion from Concordia (Table 1, Fig. 10C). Combining these first 3 results with all 4 analyses from the 2022 analytical session yields a weighted mean age of 416 ± 17 Ma (MSWD = 0.44), which is proposed as the time of magmatic crystallisation of the Crousa Downs Gabbro (early Devonian, Lochovian). As an alternative treatment, regression of the data, not corrected for common Pb (3 of the 2002 analyses and all 4 of the 2022 analyses) yield a lower Concordia intercept age of 407 ± 20 Ma (MSWD = 0.91).

In the 2002 analytical session, 6 analyses were undertaken on the 4 zircons. Zircon grain #4 with a low Th/U (Table 1), has a $^{238}U/^{206}Pb$ age of 1015 Ma, and given the very low yield of zircon grains, is regarded as a laboratory contaminant and is not considered further. The other 3 grains (3 analyses on the largest grain #1 and an analysis each on grains #2 and 3) have uniform high Th/U (>1.0) expected for mafic igneous rocks and all have similar $^{238}U/^{206}Pb$ Palaeozoic ages (Table 1; Fig. 10C). Therefore, these 3 zircons are regarded as indigenous to the sample. All analyses yield a weighted mean $^{238}U/^{206}Pb$ age of 393 ± 11 Ma (95% confidence, MSWD = 1.1), indicating some dispersion beyond

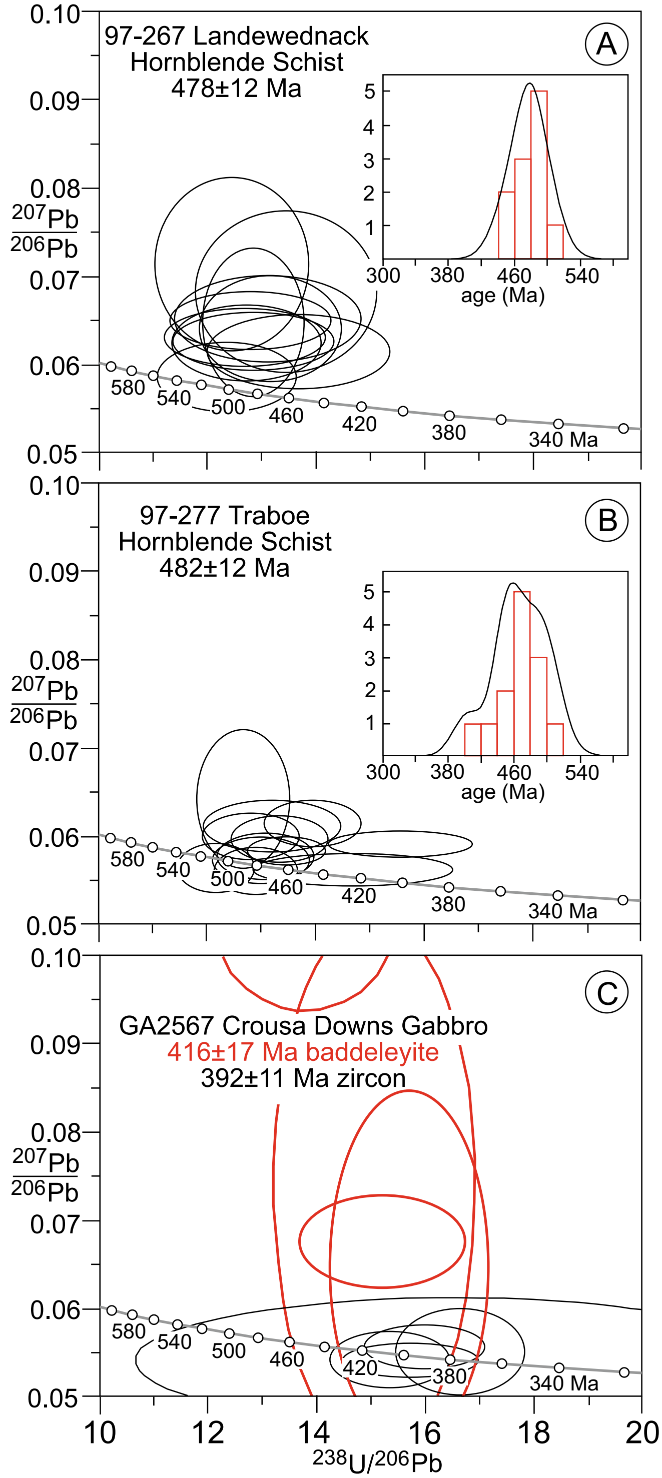

Fig. 10. $^{207}Pb/^{206}Pb$ versus $^{238}U/^{206}Pb$ Tera-Wasserburg plots (not corrected for common Pb) for samples 97-267, 97-277 and GA2567. The inserts in each Tera-Wasserburg plot are cumulate frequency distributions and histograms of the $^{206}Pb/^{238}U$ ages corrected for common Pb.

what would be expected from analytical uncertainty alone. On a model of minor loss of radiogenic Pb, rejection of analysis 1.2 yields a weighted mean $^{238}U/^{206}Pb$ age of 399 ± 13 Ma (95% confidence, MSWD = 0.5), which is interpreted as the time of zircon growth in the sample (early Devonian, Emsian).

Rather than destroy the 2 tiny baddeleyite grains from the gabbro sample, LA-ICPMS Lu-Hf isotopic analyses were undertaken on the somewhat larger ca. 399 Ma zircons (Table 2). Calculating initial ratios to 417 Ma (likely igneous age of the rock rather than the 399 Ma time of metamorphic recrystallisation), gives εHf_{417} values of +13.3 and + 15.5, and therefore fall with the range of values for model depleted mantle at that time (Fig. 6). This is additional evidence to the initial εNd value of +9.8 (Davies, 1984) for the juvenile nature of the Crousa Downs Gabbro (no evidence for contamination by older crust).

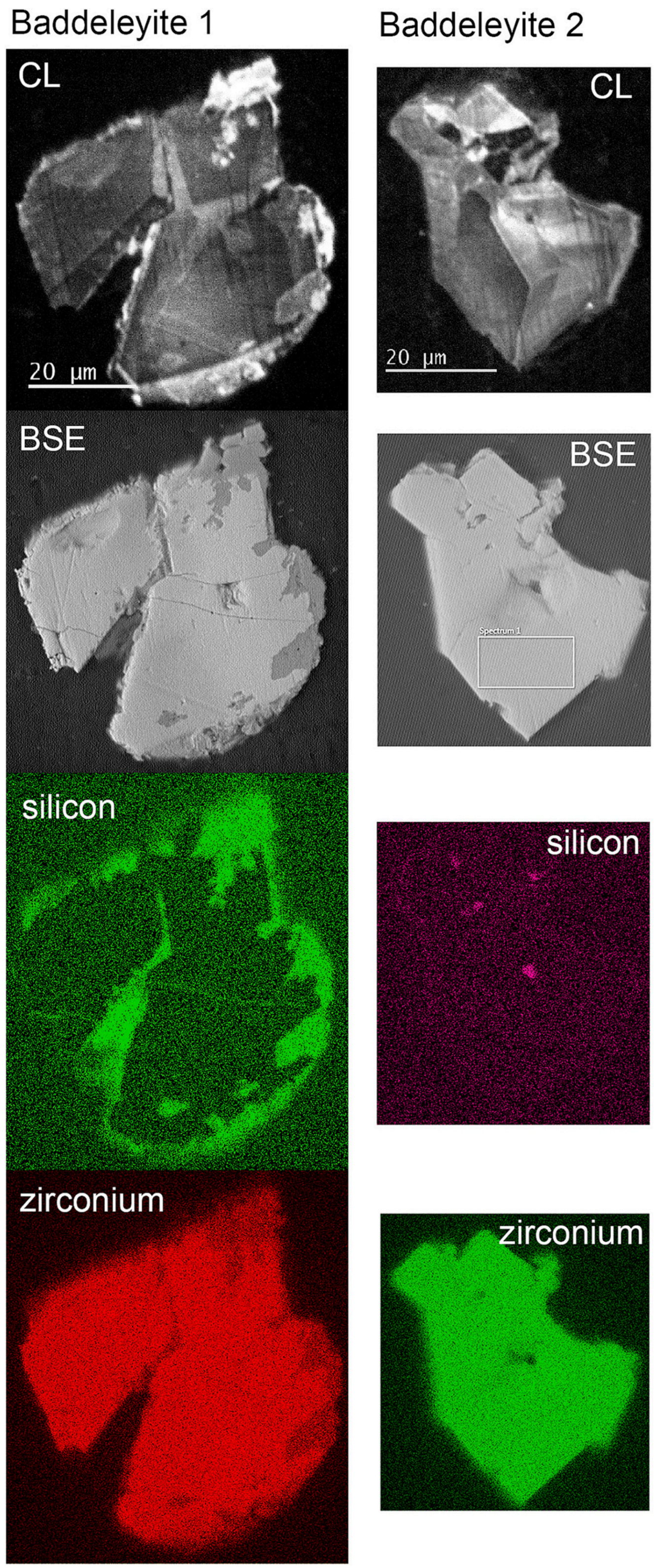

Fig. 11. Cathodoluminescence (CL), Back Scattered Electron (BSE) and silicon and zirconium maps for the 2 baddeleyite grains recovered from Crousa Downs Gabbro sample GA2567.

4.8. Pyroxene granulite felsic sheet in recrystallised peridotite, sample 96–532

Sample 96–532 is of a pyroxene granulite sheet within recrystallised lherzolite Lawarnick Pit, near Kyance (Fig. 2). Fine-grained zircons are seen in thin section. The sample yielded diverse zircons typically 100–150 μm long, which range in habit from stubby-prismatic to equant and anhedral. In CL imagery the zircons are commonly structurally diverse, but the majority of them have variably recrystallised broad to oscillatory-zoned centres, which appear rather dull in the images

(Fig. 5). Most grains also have partial outer shells, typically <10 μm wide, that appear bright in CL images. A few of the zircons have likely structural cores that are homogeneous and non-luminescent in CL imagery (Fig. 5). Sixteen U-Th-Pb analyses were undertaken on 9 zircons (Table 1, Fig. 12A). Repeat analyses were made on the structural core in grain #8 (2 analyses) and in grain #9 (5 superimposed analyses) in order to derive the best estimate of their ages. The other analyses focussed on the main population of broad to oscillatory zoned zircon. These sites display moderate U content (between 180 and 375 ppm) with Th/U ratios between 0.36 and 0.73. Prior to correction for small amounts of common Pb, all analyses yield close to concordant ages (Fig. 12A). The dominant population of broad to oscillatory-zoned zircon shows a dispersion in $^{238}U/^{206}Pb$ beyond that expected from analytical error alone. Based on a model of some radiogenic Pb loss, rejecting 4 of the 9 analyses yields a $^{238}U/^{206}Pb$ weighted mean age of 391.0 ± 10.0 Ma (MSWD = 0.92) for the remaining analyses. Given the oscillatory-zoned character of these sites, this is taken as the time of magmatic crystallisation of the sample. The highest $^{238}U/^{206}Pb$ age on the non-luminescent (high-U) cores is 485 Ma (site #9.3), which is taken as the minimum age of a xenocrystic component in the sample.

4.9. Pyroxene granulite felsic sheet in recrystallised peridotite, sample 96–558

Sample 96–558 is of a pyroxene granulite sheet within recrystallised lherzolite at Pol-Cornick, south of Predannack (Fig. 2). It gave a small yield of zircon with mostly equant with multifaceted habit, typically 200 μm across. In CL images the grains predominantly appear bright (low U + Th content) and are structureless or show weak sector zoning (Fig. 5). A small minority of the grains contain fragments of variably-recrystallised oscillatory-zoned zircon (Fig. 5). Twelve SHRIMP U-Th-Pb analyses were undertaken on 11 grains (Table 1), and all yield close to concordant ages, even prior to correction for common Pb (Fig. 12B). All analyses of the bight in CL featureless to sector-zoned zircon yield a weighted mean $^{238}U/^{206}Pb$ age of 394.0 ± 12.0 Ma (MSWD = 0.98). Analysis of relict recrystallised oscillatory zoned core #3.1 yields a marginally older age of 430 Ma.

5. Discussion: Interpretation of new zircon and baddeleyite data integrated with previous U-Pb zircon results and geological observations

5.1. Age and relationships between the Old Lizard Head Series and the Man-of-War Gneiss

The Old Lizard Head Series is intruded by a discordant granodiorite sheet with an age of 488.4 ± 9.0 Ma, whereas a concordant granodiorite layer (likely a discordant intrusion rotated into concordance by deformation) has an age of 498.9 ± 6.8 Ma. The Man-of-War Gneiss on the islets south of Lizard Head has an age of 499^{+8}_{-3} Ma (Sandeman et al., 1997) or 498 ± 11 Ma (this paper). These ages suggest that the granodiorite sheets in the Old Lizard Head Series are likely apophyses off the

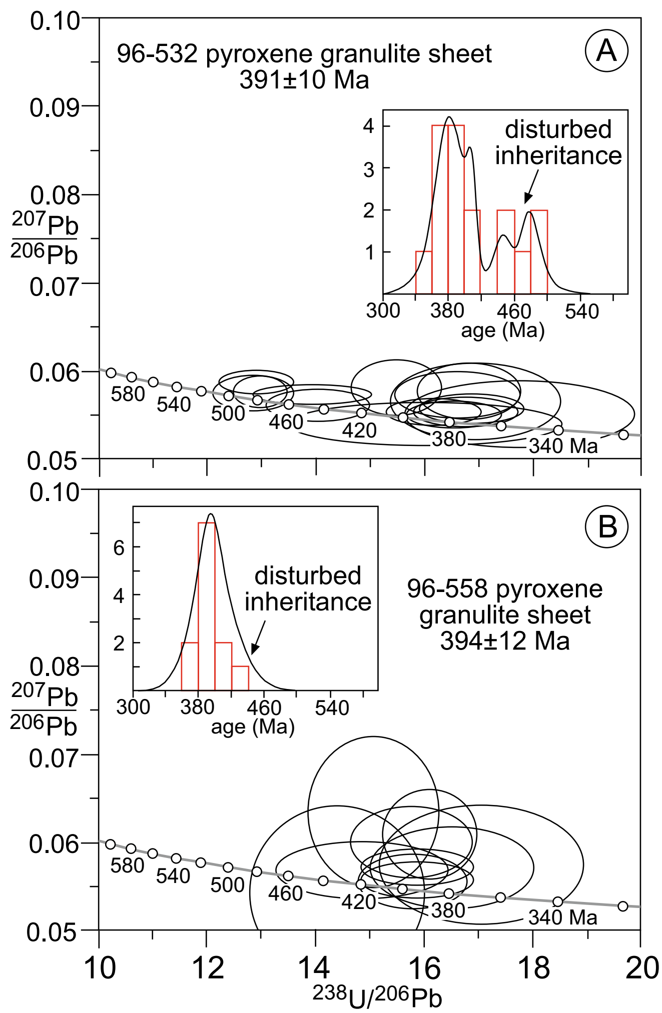

Fig. 12. $^{207}Pb/^{206}Pb$ versus $^{238}U/^{206}Pb$ Tera-Wasserburg plots (not corrected for common Pb) for samples 96–532 and 96–558. The inserts in each Tera-Wasserburg plot are cumulate frequency distributions and histograms of the $^{206}Pb/^{238}U$ ages corrected for common Pb.

main Man-of-War Gneiss. The intrusion age of 488.4 ± 9.0 Ma of a discordant granodiorite sheet constrains the age of the Old Lizard Head Series to be Miaolingian (Cambrian) or older.

5.2. Age and relationship between the Landewednack and Traboe Hornblende Schists

Both the Landewednack and the Traboe Hornblende Schists north of the Lizard Peridotite and Crousa Down Gabbro have small yields of small stubby prismatic to equant zircons with relict oscillatory zoning and unimodal ages of 478.0 ± 12 and 482.0 ± 12 Ma respectively. Samples from these northerly occurrences have narrow recrystallisation rims which are bright (low U + Th) in CL images (Fig. 5), but are too narrow to be analysed by a ca. 20 μm spot. On the south side of the peridotite near Lizard Head, a pelitic schist unit within the Landewednack Hornblende Schists gave a small yield of zircons, some with broader metamorphic overgrowths / recrystallisation rims. The cores and whole grains yield ages from ca. 490 up to 735 Ma, and are interpreted are a small detrital component from Cambrian to Neoproterozoic sources. Combining the metamorphic age rim determinations from the pelitic sample 96–546 (this paper) with the low U, low Th/U metamorphic grains in hornblende schist sample 96–543 from the same locality (Nutman et al., 2001), yields a spread in ^{238}U/^{206}Pb ages beyond that expected from analytical uncertainty. These ages appear to be bimodal and mixture modelling of the data extracts two populations of 407 ± 14 and 361 ± 22 Ma, pointing to imprinting from more than one tectonothermal event. The presence of 478 to ca. 490 Ma magmatic-sourced grains in all samples indicate that if this is a volcano-sedimentary component, the likely protolith age of these schists is latest Cambrian to earliest Ordovician, and therefore younger than the Old Lizard Head Series, which must be Miaolingian (Cambrian) or older, because it is cut by ca. 500 Ma granodiorite sheets (Fig. 4). Additionally, the presence of Neoproterozoic detrital grains in pelite schist sample 97-546 demonstrates the proximity of older (continental) crust at the time that the Landewednack and Traboe Hornblende Schist protoliths formed. Although they have indistinguishable formation ages, this does not mean they had exactly the same protoliths, with for example Floyd et al. (1993) suggesting the Landewednack Hornblende Schists have a volcanic provenance (in keeping with the presence of pelitic layers), whereas the Traboe Hornblende Schists have a plutonic origin. Furthermore, from data in Leake and Styles (1984), the Traboe Hornblende Schists have low Ti/V in the range found in arc-related rocks, whereas the Landewednack Hornblende Schists have higher Ti/V in the range expected for back-arc basin rocks and MORB.

5.3. Ages and relationship between the Traboe Hornblende Schist and the Crousa Downs Gabbro

Rare baddeleyite recovered from the Crousa Downs Gabbro has a U-Pb age of 417 ± 16 Ma, which is interpreted here as the time of magmatic crystallisation. Despite the large uncertainty on this age determination, it is older than previous age determinations, such as the Sm-Nd mineral isochron of 375 ± 34 Ma (Davies, 1984) which was ascribed to an episode of post-magmatic metamorphic recrystallisation. SEM elemental mapping (Fig. 11) shows that the rare baddeleyite grains are partially recrystallised to zircon, demonstrating a post magmatic event. Rare zircons from the Crousa Downs Gabbro have a U-Pb age of 393 ± 11 Ma, and is in accord with previous age determinations (e.g., Davies, 1984) interpreted as post-400 Ma metamorphic recrystallisation. It should also be noted that the age of the Crousa Downs Gabbro metamorphic zircons is in accord with the age of the Kennack Gneiss, pyroxene granulite sheets in the Lizard Peridotite and metamorphic zircon growth in the Traboe and Landewednack Hornblende Schists (Fig. 4). The U-Th-Pb zircon and baddeleyite data presented in this paper demonstrate that the Traboe Hornblende Schist and the Crousa Downs Gabbro are different in age by probably ca. 80 million years and thus are unrelated (Fig. 4). The ca. 417 Ma baddeleyite age (early Devonian – Lochovian) for the Crousa Downs Gabbro marks a late stage extensional magmatic event in an ephemeral rift proposed in some syntheses (e.g., Floyd, 1984; Cook et al., 2002; Zeh and Will, 2010; Leveridge and Shail, 2011).

5.4. Crustal thickening following basin inversion

The Old Lizard Head series is described as containing the metamorphic indicator minerals cordierite, staurolite, andalusite, sillimanite and kyanite (Flett, 1946; Tilley, 1937). Clearly, the listing of cordierite and sillimanite/andalusite versus kyanite indicates polybaric conditions, with the kyanite an indication of an episode of higher pressure metamorphism. On the other hand, staurolite indicates some metamorphic recrystallisation took place in a temperature range of ca. 550–650 °C.

Another indication of the crustal thickening during basin inversion is the new zircon REE evidence that magmatic bodies (sample 96–532, this paper) emplaced into the peridotite shortly after 400 Ma had equilibrated with garnet during their ascent. This is given by the weak enrichment in the heavy REE (ca. 100 to 200 times chondrite), rather than the typical 5000 to 10,000 times chondrite for magmatic zircons that did not equilibrate with garnet (Fig. 7).

The age of the Crousa Downs Gabbro metamorphic zircons is in accord with the magmatic age of the Kennack Gneiss, pyroxene granulite sheets in the Lizard Peridotite and metamorphic zircon growth in the Traboe and Landewednack Hornblende Schists (Fig. 4). The pyroxene-bearing rocks are coeval with the Kennack Gneiss. Supported by the occurrence of pre-magmatic zircon and the Hf isotopic data we contend that these bodies are also melts formed below the Lizard Complex, but crystallised in an ambient higher temperature environment (giving rise to them carrying pyroxene rather than biotite +/− hornblende). Inversion can now be placed within the period 416 ± 17 to 397 ± 7 Ma – the age of the Crousa Downs Gabbro and the 'oldest' granite vein (Fig. 4; Lochkovian-Emsian). This is slightly earlier than some previous estimates, such as 390–375 Ma (Cook et al., 2002; Eifelian-Frasnian). Combining all the post-400 Ma SHRIMP age determinations gives a weighted mean ^{202}Pb/^{238}U age of 388.1 ± 3.7 (95% confidence, MSWD = 1.6). If the high MSWD is due to some radiogenic Pb-loss from samples 96/530 and 97/713 zircons, then culling these samples gives a mean age of 391.2 ± 3.3 Ma (MSWD = 0.79) for a single 'hot' thermal event. Alternatively, mixture modelling of the post-400 Ma ages reveals two populations closely spaced in age of 384.9 ± 3.3 Ma and 392.0 ± 4.4 Ma (2σ; 38% and 62% of population respectively). There is in all likelihood complexity in the post inversion tectonothermal history, as outlined by some previous studies such as Cook et al. (2002), who proposed an early 'hot' emplacement event at 390–375 Ma, followed by a 'cold' second phase at ca. 365 Ma.

5.5. Terrane affinity of the rocks structurally below the Lizard Peridotite

The zircon dating presented in Sandeman et al. (1997), Nutman et al. (2001) and this paper demonstrate that the Lizard Peridotite is bounded to the south and underlain by Cambrian rocks, which contain older zircon components dating back to the Palaeoproterozoic (Figs. 4 and 9). Thus, pre-500 Ma zircons have been found in Landewednack Hornblende Schist metapelite sample 96–546, inherited zircon cores in Kennack Gneiss samples 96–513, −514 and 97-517 and inherited zircon cores in pyroxene granulite sheets 96–530, −532 and − 558 (Nutman et al., 2001 and this paper). These total 22 analyses on 19 grains, and their age probability distribution is presented in Fig. 13 where it is compared and contrasted with the ages of both the (i) Normanian terrane as exposed in Normandy at the southern edge of the Trégor-La Hague Terrane (sample AM 1) and (ii) with the Devonian Gramcatho Basin wild flysch of the Meneage Formation (sample Liz 3; Strachan et al., 2014). Zircons analysed from all three of these have a distinctive

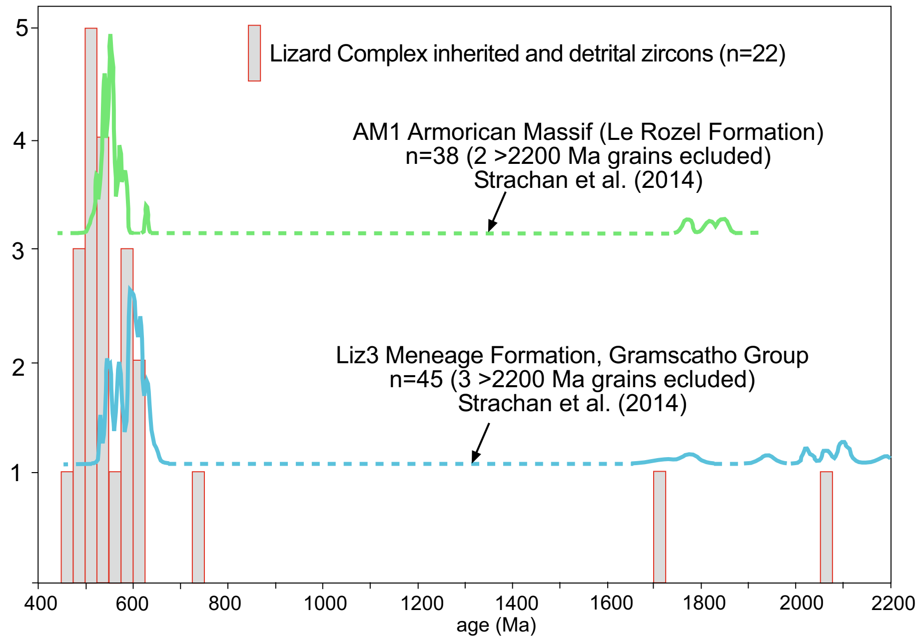

Fig. 13. Pre-Lizard Complex inherited and detrital zircon ages compared with AM1 (Amorican Massif) and Liz3 (Meneage Formation) from Strachan et al. (2014).

bimodal age distribution, dominated by a late Neoproterozoic to middle Cambrian (ca. 735–502 Ma) with a lesser Palaeoproterozoic (ca. 1800–2200 Ma) grouping (Fig. 13). This age distribution closely resembles the age of lithologies and detrital zircons exposed in Armorica to the south of English Channel (Fig. 1; data compilation from Drost et al., 2011; Linnemann et al., 2004, 2008), in terranes regarded of Gondwanan affinity. On the other hand, the scarcity of Mesoproterozoic (1000–1600 Ma) zircons is in marked contrast to the abundance of this age grouping linked to East Avalonia (e.g., Collins and Buchan, 2004; Samson et al., 2005), which forms the basement between southern England and the Iapetus suture passing through Ireland and northernmost England (Fig. 1). We therefore conclude that these rocks represent part of the Normanian (Armorican) terrane and are not part of Avalonia.

5.6. Does the Lizard Complex mark the Avalonia-Armorica suture or an intra-Armorican basin?

In early tectonic syntheses, the Lizard Complex, along with the Start Point rocks of south Devon (Fig. 1) were interpreted as a final suture between Laurentian Avalonia to the north and Gondwanan Armorica to the south (Wilson, 1966 and see Fig. 2 in Murphy et al., 2006). Accruing evidence is reducing the likelihood of this scenario. For example, the geochemical study of Permian lamprophyres in southwest England (Dijkstra and Hatch, 2018) indicates that Armorican basement and lithospheric mantle continue beyond the Lizard – Start Point line and a suture with the Avalon terrane is likely hidden at depth farther north, under the Devonian-Carboniferous Variscan fold and thrust belt (northern Rheic Ocean suture? on Fig. 1). This interpretation places the first joining of some Gondwanan crustal fragments with Avalonia as pre-Devonian, earlier in the Palaeozoic. This contrasts with models that interpret the Lizard Complex as marking suturing, which would place it significantly later at the Silurian-Devonian boundary.

Alternatively, many workers now interpret the Lizard Complex and the Start Point rocks as vestiges of a rift (commonly referred to in the literature as the Rheno-Hercynian Ocean) within a single terrane, rather than marking closure of an extensive ocean. For example, Davies (1984) likened the development of the Lizard Complex to a closed narrow seaway like the Red Sea. This seaway was extended far to the east by Zeh and Will (2010), who regarded the Giessen back arc assemblage of the mid-German Crystalline Zone as related to a rift now marked by the Lizard Complex. Detailed analysis of early fabrics (Roberts et al., 1993) in the Lizard Peridotite proposed localized NE-SW rifting in a pull-apart basin setting (Cook et al., 2002). A common definition of ophiolite is ‘Ophiolites are portions of ancient ocean floors carried onto a continent due to collision between continents or between a continent and an arc’. Thus using the word ‘ophiolite’ can lead to a common perception that a ‘wide’ ocean has closed. This is an idea that we authors, as well as some other researchers, would want to avoid when it comes to the Lizard Complex. Instead, there is the case made (again, not only by ourselves) that the Lizard Complex represents a narrow seaway, perhaps like the Red Sea, that was short-lived. For this reason we wish not to refer it as an ophiolite, without qualification.

5.7. Contemplations on the demise of the Rheic Ocean

If the Rheic Ocean had fragments of Gondwanan basement scattered within it (e.g., Alexander et al., 2019 and references therein), then expecting a single date for the closure of all of this ocean is not a reality. Instead, each suture marked by ophiolites sensu stricto, ultramafic-mafic assemblages such as the Lizard Complex and by eclogite and blueschist facies high pressure metamorphism, are events recording when rifts and oceanic domains closed, and when ribbons of peri-Gondwanan crust docked with Avalonia / Baltica or were reunited with Gondwana (Fig. 1). Given this perspective, then ocean demise will be given by the youngest of such events.

Accepting a narrow, short-lived rift interpretation for the Lizard Complex, then southwest England (i.e. north of the Lizard Complex) is an Armorican fragment of Gondwanan affinity that, prior to the Devonian, had docked earlier with Avalonia / Baltica by closure of a northern strand of the Rheic Oceans (e.g., Zeh and Will, 2010; Franke et al., 2017; Alexander et al., 2019). Evidence for this cryptic suture is given by geochemical changes of Permian lamprophyres north-south across southwest England, which demonstrates contrasting deep lithosphere (Dijkstra and Hatch, 2018; see boundary marked as cryptic early northern Rheic Ocean suture? on Fig. 1). Such a scenario finds parallel in the history of Tethys, where in Iraq-Iran the Gondwanan Sanandaj-Sirjan Zone docked with Eurasia in the Jurassic, prior to the final closure of Tethys in the Cenozoic, when the Arabian microcontinent docked against Eurasia (e.g., Ali et al., 2019; Fergusson et al., 2016 and references therein). Therefore, in the interpretation for the Lizard

Complex as marking the inversion of a narrow short lived rift in the early Devonian, the suture zone or zones marking demise of the Rheic Ocean should lie south of the Lizard Complex, beyond the Normanian terrane / nappe (Fig. 1). In northern Brittany on the south side of the English Channel, the Léon Domain marks the southern margin of the Normanian Terrane (Fig. 1) and contains partially retrogressed eclogites which may have formed as early as ca. 440 Ma (early Silurian) or possibly later (Schultz et al., 2007). Farther south, the Massif Central domain between the Central- and the South Armorican domains (Fig. 1) is marked by several eclogite and blueschist occurrences occurring along with ophiolitic rocks (reviewed by Ballèvre et al., 2009), with both ca. 410–390 and 370 to 360 Ma ages for high pressure metamorphism (U-Pb monazite, zircon and Ar-Ar phengite respectively; Bosse et al., 2000). This zone continues eastwards into the Moldanubian in central Europe which contains relicts of high pressure metamorphism with a range of 350–330 Ma ages (e.g., Beard et al., 1992; Kröner et al., 2000; Prince et al., 2000). To the west, the same domain is considered to occur in the Iberian Galicia-Trás-os-Montes and the Ossa-Morenza Zones (reviewed in Murphy et al., 2016), where relicts of high pressure metamorphism again have ages such as 340 Ma for metamorphic zircon (e.g., Ordóñez Casado, 1998) with retrogression by 330 Ma recorded by Ar/Ar mica (e. g., Quesada and Dallmeyer, 1994). South of this tract stretching from Iberia to central Europe, Gondwanan basement is devoid of structural lineaments bearing relicts of Hercynian eclogites, blueschists or ophiolitic assemblages. The 350–330 Ma high pressure metamorphism occurrences are the youngest associated with the Hercynides, and thus point to demise of the last parts of the Rheic Ocean in the middle Carboniferous, at least 50 million years after the initial thrusting of the Lizard Complex over the Devonian Gramscatho Basin.

Thus as demonstrated by other workers, the demise of the Rheic Ocean was via several docking events from perhaps the Ordovician-Silurian at ≥440 Ma (e.g., Schultz et al., 2007; Zeh and Will, 2010; Dijkstra and Hatch, 2018; Alexander et al., 2019) through to the middle Carboniferous (ca. 330 Ma), as marked by the youngest high pressure metamorphism (e.g., as summarised in Ballèvre et al., 2009 and Murphy et al., 2016). However, ca. 330 Ma did not mark the end of convergence and deformation in the Hercynides. For example, the youngest deformed rocks in the Culm Basin (Fig. 1) of southwest England are the Westphalian C (≈ Kasimovian) Bude Formation which is unconformable below the uppermost Carboniferous to Permian Exeter Group, demonstrating that convergent deformation there lasted up to ca. 304 Ma (Edwards et al., 1997).

6. Conclusions

(1) Dating of intrusive granodiorite sheets at ca. 500 Ma constrain the age of their host Old Lizard Head rocks to Miaolingian (Cambrian) or older. These sheets are likely apophyses of the Man-of-War Gneiss.

(2) The zircon geochronology on the Landewednack Hornblende Schists and the Traboe Hornblende Schists show that they have an age of 480–470 Ma (Ordovician). Therefore, the Traboe Hornblende Schists are significantly older than, and unrelated to, the Crousa Downs Gabbro (Devonian).

(3) Detrital zircon dating of a metapelite in the Landewednack Hornblende Schists demonstrates a southern, Normanian Terrane (Armorican) provenance.

(4) The Crousa Downs Gabbro is demonstrated by U-Pb dating of baddeleyite to be slightly older than 400 Ma. Hf isotopic analysis demonstrates it to be uncontaminated by older crust, as suggested by previous whole rock Nd isotopic studies (Davies, 1984).

(5) The inversion of the rift which the Lizard Complex marks was as early as 400–395 Ma, slighter earlier than previously proposed and very soon after the Crousa Downs Gabbro was intruded.

(6) Zircon Hf isotopic and REE signatures of zircon in the felsic granulite sheets intruded into the Lizard Peridotite add extra evidence that by 400–395 Ma the Lizard Peridotite with the juvenile Crousa Downs Gabbro were underlain by felsic crust undergoing garnet-grade metamorphism.

(7) The new data indicate that the Lizard Complex closed approximately 80 million years prior to the demise of the entire Rheic Ocean. This supports previous syntheses (e.g., Floyd, 1984; Cook et al., 2002; Leveridge and Shail, 2011) that the Lizard Complex does not mark a final Rheic suture.

Declaration of Competing Interest

The authors declare that they have no known competing financial interests or personal relationships that could have appeared to influence the work reported in this paper.

Acknowledgement

Shane Paxton is thanked for careful heavy mineral separations. Thoughtful and constructive reviews by Rob Strachan and Robin Shail were much appreciated.

Appendix A. Supplementary data

Supplementary data to this article can be found online at https://doi.org/10.1016/j.lithos.2023.107227.

References

Alexander, A.C., Shail, R.K., Leveridge, B.E., 2019. Late Paleozoic extensional reactivation of the Rheic–Rhenohercynian suture zone in SW England, the English Channel and Western Approaches. Geol. Soc. Lond. Spec. Publ. 470, 353.
Ali, S.A., Nutman, A.P., Aswad, K.J., Jones, B.G., 2019. Overview of the tectonic evolution of the Iraqi Zagros thrust zone: sixty million years of Neotethyan subduction. J. Geodyn. 129, 162–177. https://doi.org/10.1016/j.jog.2019.03.007.
Ballèvre, M., Basse, V., Ducassou, C., Pitra, P., 2009. Palaeozoic history of the Armorican Massif: Models for the tectonic evolution of the suture zones. Compt. Rendus Geosci. 341, 174–201.
Barnes, R.P., Andrews, J.R., 1984. Hot or cold emplacement of the Lizard Complex? J. Geol. Soc. Lond. 141, 37–40.
Beard, B.L., Medaris, L.G., Johnson, C.M., Brueckner, K.H., Mísař, Z., 1992. Petrogenesis of Variscan high-temperature Group A eclogites from the Moldanubian Zone of the Bohemian Massif, Czechoslovakia. Contrib. Mineral. Petrol. 111, 468–483.
Black, L.P., Kamo, S.L., Allen, C.M., Aleinikoff, J.N., Davis, D.W., Korsch, R.J., Foudoulis, C., 2003. TEMORA 1: a new zircon standard for Phanerozoic U–Pb geochronology. Chem. Geol. 200, 155–170.
Bosse, V., Féraud, G., Ballèvre, M., Peucat, J.-J., de Jong, K., 2000. Late Devonian subduction and early orogenic exhumation of eclogite-facies rocks from the Champtocaeux complex (Variscan belt, France). Geol. J. 35, 297–325.
Bouvier, A., Vervoort, J.D., Patchett, J., 2008. The Lu–Hf and Sm–Nd isotopic composition of CHUR: constraints from unequilibrated chondrites and implications for the bulk composition of the terrestrial planets. Earth Planet. Sci. Lett. 273, 48–57.
Bromley, A.V., 1975. Is the Lizard Complex, South Cornwall, a fragment of Hercynian Ocean crust? Lizard 5, 2–11.
Bromley, A.V., 1979. Ophiolitic origin of the Lizard complex. Cambourne School Mines J. 79, 25–38.
Clark, A.H., Sandeman, H.A.I., Nutman, A.P., Green, D.H., Cook, A., 2003. Discussion on SHRIMP U–Pb zircon dating of the exhumation of the Lizard Peridotite and its emplacement over crustal rocks: constraints for tectonic models. J. Geol. Soc. Lond. 160, 331–335.
Cocks, L.R.M., Fortey, R.A., 1982. Faunal evidence for oceanic separations in the Palaeozoic of Britain. J. Geol. Soc. Lond. 139, 456–478.
Cocks, L.R.M., Fortey, R.A., 1990. Biogeography of Ordovician and Silurian faunas. In: McKerrow, W.S., Scotese, C.R. (Eds.), Palaeozoic Palaeogeography and Biogeography, Geological Society London Memoir, 12, pp. 97–104.
Collins, A.S., Buchan, C., 2004. Provenance and ago constraints of the South Stack Group, Anglesey, UK: U–Pb SIMS detrital zircon data. J. Geol. Soc. Lond. 161, 743–746.
Compston, W., Williams, I.S., Myer, C., 1984. U-Pb geochronology of zircons from lunar breccia 73217 using a sensitive high mass-resolution ion microprobe. J. Geophys. Res. 89B, 525–534.
Cook, C.A., Holdsworth, R.E., Styles, M.T., 1998. The tectonic evolution of peridotites in the Lizard complex, south-west England. Geosci. South-west England 8, 182–187.
Cook, C.A., Holdsworth, R.E., Styles, M.T., Pearce, J.A., 2000. Pre-emplacement structural history recorded by mantle peridotites: an example from the Lizard Complex, SW England. J. Geol. Soc. Lond. 157, 1049–1064.
Cook, C.A., Holdsworth, R.E., Styles, M.T., 2002. The emplacement of peridotites and associated oceanic rocks from the Lizard Complex, southwest England. Geol. Mag. 139, 27–45. https://doi.org/10.1017/S0016756801005933.

Cumming, J.L., Richards, J., 1975. Ore lead ratios in a continuously changing Earth. Earth Planet. Sci. Lett. 28, 155–171.
Davies, G.R., 1984. Isotopic evolution of the Lizard complex. J. Geol. Soc. Lond. 141, 3–14.
Dijkstra, A.J., Hatch, C., 2018. Mapping a hidden terrane boundary in the mantle lithosphere with lamprophyres. Nat. Commun. 9, 3770.
Drost, K., Gerdes, A., Jeffries, T., Linnemann, U., Storey, C., 2011. Provenance of Neoproterozoic and early Palaeozoic siliciclastic rocks of the Teplá-Barrandian unit (Bohemian Massif); evidence from U-Pb detrital zircon ages. Gondwana Res. 19, 213–123.
Edwards, R.A., Warrington, G., Scrivener, R.C., Jones, N.S., Haslam, H.W., Ault, L., 1997. The Exeter Group, south Devon, England: a contribution to the early post-Variscan stratigraphy of Northwest Europe. Geol. Mag. 134, 177–197.
Eggins, S.M., Rudnick, R.L., McDonough, W.F., 1998. The composition of peridotites and their minerals: a laser ablation ICP-MS study. Earth Planet. Sci. Lett. 154, 53–71.
Fergusson, C., Nutman, A.P., Mohajjel, M., Bennett, V.C., 2016. The Sanandaj-Sirjan Zone in the Neo-Tethyan suture, western Iran: zircon U-Pb evidence of late Palaeozoic rifting of northern Gondwana and mid Jurassic orogenesis. Gondwana Res. 40, 43–57. https://doi.org/10.1016/j.gr.2016.08.006.
Flett, J.S., 1946. The Geology of the Lizard and Meneage (Sheet 359). Memoir of the Geological Survey of Great Britain, 2nd edition. HMSO, London.
Flett, J.S., Hill, J.B., 1912. The Geology of the Lizard and Meneage. Memoir of the Geological Survey of Great Britain, 1st edition. HMSO, London.
Floyd, P.A., 1984. Geochemical characteristics and comparison of the basic rocks of the Lizard Complex and the basaltic lavas within the Hercynian troughs of SW England. J. Geol. Soc. Lond. 141, 61–70.
Floyd, P.A., Exley, C.S., Styles, M.T., 1993. Igneous Rocks of South-West England. Geological Conservation Review Series. Chapman and Hall, London.
Franke, W., 1989. Variscan plate-tectonics in Central Europe - current ideas and open questions. Tectonophysics 169, 221–228.
Franke, W., Cocks, L.R.M., Torsvik, T.H., 2017. The Palaeozoic Variscan oceans revisited. Gondwana Res. 48 (1982).
Green, D.H., 1964a. The petrogenesis of the high temperature peridotite intrusion in the Lizard area, Cornwall. J. Petrol. 5, 134–188.
Green, D.H., 1964b. The metamorphic aureole of the peridotite at the Lizard, Cornwall. J. Geol. 5, 134–188.
Green, D.H., 1964c. A re-study and re-interpretation of the geology of the Lizard Peninsula, Cornwall. Hosking, K.F.G. and Shrimpton, G.J., Present views on some aspects of the geology of Cornwall and Devon. Royal Geological Society of Cornwall, In, pp. 87–114.
Heaman, L.M., 2009. The application of U-Pb geochronology to mafic, ultramafic and alkaline rocks: an evaluation of three mineral standards. Chem. Geol. 261, 42–51.
Hiess, J., Bennett, V.C., Nutman, A.P., Williams, I.S., 2009. In situ U-Pb, O and Hf isotopic compositions of zircon from Eoarchaean tonalite and felsic volcanic rocks, Itsaq Gneiss complex, southern West Greenland: new constraints on the source materials for the early crust. Geochim. Cosmochim. Acta 73, 4489–4516.
Holder, M.T., Leveridge, B.E., 1986. A model for the tectonic evolution of south Cornwall. J. Geol. Soc. Lond. 143, 125–134.
Jones, K.A., 1994. The most southerly point thrust - an example of ductile thrusting in the Lizard Complex, SW Cornwall. Proc. Usher Soc. 8, 254–261.
Jones, K.A., 1997. Deformation and emplacement of the Lizard Ophiolite Complex, SW England, based on evidence from the Basal Unit. J. Geol. Soc. Lond. 154, 871–885.
Kirby, G.A., 1979. The Lizard Complex as an ophiolite. Nature 282, 58–61.
Kröner, A., O'Brien, P.J., Nemchin, A.A., Pidgeon, R.T., 2000. Zircon ages for high pressure granulites from the South Bohemia, Czech Republic, and their connection to Carboniferous high temperature processes. Contrib. Mineral. Petrol. 138, 127–142.
Leake, R.C., Styles, M.T., 1984. Borehole sections through the Traboe hornblende schists, a cumulate complex overlying the Lizard peridotite. J. Geol. Soc. Lond. 141, 41–52.
Leveridge, B.E., Shail, R.K., 2011. The Gramscatho Basin, South Cornwall, UK: Devonian active margin successions. Proc. Geol. Assoc. 122, 568–615.
Leveridge, B.E., Hartley, A.J., 2006. The Variscan Orogeny: The development and deformation of Devonian/Carboniferous basins in SW England and South Wales. In: Brenchley, P.J., Rawson, P.F. (Eds.), The Geology of England and Wales. Geological Society of London, London, pp. 225–255.
Linnemann, U., McNaughton, N.J., Romer, R.L., Gehmlich, M., Drost, K., Tonk, C., 2004. West African provenance for Saxo-Thuringia (Bohemian Massif): did Armorica ever leave pre-Pangean Gondwana? U-Pb SHRIMP zircon evidence and the Nd isotopic record. Int. J. Earth Sci. 93, 683–705.
Linnemann, U., D'Lemos, R.S., Drost, K., Jeffries, T., Gerdes, A., Romer, R.L., Samson, S. D., Strachan, R.A., 2008. Cadomian tectonics. In: McCann, T. (Ed.), The Geology of Central Europe, volume 1: Precambrian and Palaeozoic. Geological Society of London, pp. 103–154.
Ludwig, K., 1998. Isoplot/Ex. Berkeley Geochronology Center, Publication 1.
Murphy, J.B., Gutiérrez-Alonso, G., Nance, R.D., Fernández-Suáez, J., Keppie, J.D., Quesada, C., Strachan, R.A., Dostal, J., 2006. Origin of the Rheic Ocean: rifting along a Neoproterozoic suture? Geology 32, 585–588.
Murphy, J.B., Quesada, C., Gutiérrez-Alonso, G., Johnston, S.T., Weil, A., 2016. Reconciling competing models for the tectono-stratigraphic zonation of the Variscan orogen in Western Europe. Tectonophysics 681, 209–219.
Norman, M.D., Pearson, N.J., Sharma, A., Griffin, W.L., 1996. Quantitative analysis of trace elements in geological materials by laser ablation ICPMS: instrumental operating conditions and calibration values for NIST glasses. Geostand. Newslett. 20, 247–261.
Nutman, A.P., Green, D.H., Cook, C.A., Styles, M.T., Holdsworth, R.E., 2001. SHRIMP U/Pb zircon dating of the exhumation of the Lizard Peridotite and its emplacement over crustal rocks, Cornwall, England: constraints for tectonic models. J. Geol. Soc. Lond. 158, 809–820.
Ordóñez Casado, B., 1998. Geochronological studies of the Pre-Mesozoic basement of the Iberian Massif: The Ossa-Morena zone and the allochthonous complexes within the Central Iberia Zone. Dissertation ETH-Zürich.
Power, M.R., Alexander, A.C., Shail, R.K., Scott, P.W., 1996. A re-interpretation of the internal structure of the Lizard Complex ophiolite, south Cornwall. Proc. Ussher Soc. 9, 63–67.
Prince, C.I., Košler, J., Vance, D., Günther, D., 2000. Comparison of laser ablation ICP-MS and isotope dilution REE analyses – implications for Sm–Nd garnet geochronology. Chem. Geol. 168, 255–274.
Quesada, C., Dallmeyer, R.D., 1994. Tectonothermal evolution of the Badajoz-Córdoba shear zone (SW Iberia): characteristics and $^{40}Ar/^{39}Ar$ mineral age constraints. Tectonophysics 231, 195–213.
Rattey, P.R., Sanderson, D.J., 1984. The structure of SW Cornwall and its bearing on the emplacement of the Lizard Complex. J. Geol. Soc. Lond. 141, 87–95.
Roberts, S., Andrews, J.R., Bull, J.M., Sanderson, D.J., 1993. Slow-spreading ridge-axis tectonics: evidence from the Lizard Complex, UK. Earth Planet. Sci. Lett. 116, 101–112.
Rubatto, D., Williams, I.S., Buick, I.S., 2001. Zircon and monazite response to prograde metamorphism in the Reynolds Range, central Australia. Contrib. Mineral. Petrol. 140, 458–468.
Samson, S.D., D'Lemos, R.S., Miller, B.V., Hamilton, M.A., 2005. Neoproterozoic palaeogeography of the Cadomia and Avalon terranes: constraints from U-Pb ages. J. Geol. Soc. Lond. 162, 65–71.
Sandeman, H.A., Clark, A.H., Styles, M.T., Scott, D.J., Malpas, J.G., Farrar, E., 1997. Geochemistry and U-Pb and $^{40}Ar/^{39}Ar$ geochronology of the Man of War Gneiss, Lizard Complex, SW England: pre-Hercynian arc-type crust with a Sudeten-Iberian connection. J. Geol. Soc. Lond. 154, 403–417.
Sandeman, H.A., Clark, A.H., Scott, D.J., Malpas, J.G., 2000. The Kennack Gneiss of the Lizard peninsula, Cornwall, SW England: comingling and mixing of mafic and felsic magmas accompanying Givetian continental incorporation of the Lizard ophiolite. J. Geol. Soc. Lond. 157, 1227–1242.
Scherer, E., Munker, C., Mezger, K., 2001. Calibration of the lutetium–hafnium clock. Science 293, 683–687. https://doi.org/10.1126/science.1061372.
Schultz, B., Krenn, E., Finger, F., Brätz, H., Klemd, R., 2007. Cadomian and Variscan metamorphic events in the Léon domain (Armorican Massif, France): P-T data and EMP monazite dating. In: Linnemann, U., Nance, R.D., Kraft, P., Zulauf, G. (Eds.), The evolution of the Rheic Ocean: from Avalonian-Codomian active margin to the Alleghenian-Variscan collision, Geological Society of America Special Paper 423, pp. 267–285.
Shail, R.K., Leveridge, B.E., 2009. The Rhenohercynian passive margin of SW England: Development, inversion and extensional reactivation. Compt. Rendus Geosci. 341, 140–155.
Söderlund, U., Patchett, P.J., Vervoort, J.D., Isachsen, C.E., 2004. The ^{176}Lu decay constant determined by Lu–Hf and U–Pb isotope systematics of Precambrian mafic intrusions. Earth Planet. Sci. Lett. 219, 311–324. https://doi.org/10.1016/S0012-821X(04)00012-3.
Steiger, R.H., Jäger, E., 1977. Subcommission on geochronology: convention on the use of decay constants in geo- and cosmochronology. Earth Planet. Sci. Lett. 36, 359–362.
Stern, R.A., 1998. High-resolution SIMS determination of radiogenic trace-isotope ratios in minerals. In: Cabri, L.J., Vaughan, D.J. (Eds.), Modern Approaches to Ore and Environmental Mineralogy, Mineralogical Association of Canada Short Course Series, 27, pp. 241–268.
Strachan, R.A., Linnemann, U., Jeffries, T., Drost, K., Ulrich, J., 2014. Armorican provenance of the mélange deposits below the Lizard ophiolite (Cornwall, UK): evidence for Devonian obduction of Cadomian and Lower Proterozoic crust onto the southern margin of Avalonia. Int. J. Earth Sci. 103, 1359–1383.
Styles, M.T., Kirby, G.A., 1980. New Investigations of the Lizard Complex, Cornwall, England and a discussion of an ophiolite model. Ophiolites: Proceedings of the International Symposium, Cyprus, 1979. Geological Survey Department, Nicosia, pp. 512–526.
Tilley, C.E., 1937. Anthophyllite-cordierite granulites of the Lizard. Geol. Mag. 74, 300–309.
Vearncombe, J.R., 1980. The Lizard ophiolite and two phases of suboceanic deformation. In: Panayiotou, A. (Ed.), Ophiolites: Proceedings of the International Symposium, Cyprus, 1979. Geological Survey Department, Nicosia, pp. 527–537.
White, L.F., Tait, K.T., Kamo, S.L., Moser, D.E., Darling, J.R., 2020. Highly accurate dating of micrometre-scale baddeleyite domains through combined focused ion beam extraction and U–Pb thermal ionization mass spectrometry (FIB-TIMS). Geochronology 2, 177–186. https://doi.org/10.5194/gchron-2-177.
Williams, I.S., 1998. U-Th-Pb geochronology by ion microprobe. In: McKibben, M.A., Shanks III, W.C.P., Ridley, W.I. (Eds.), Applications of Microanalytical Techniques to Understanding Mineralizing Processes. Society of Economic Geologists Short Course, 7.
Wilson, J.T., 1966. Did the Atlantic close and then re-open? Nature 211, 676–681.
Zeh, A., Will, T.M., 2010. The Mid-German Crystalline Rise. In: Linnemann, U., Romer, R. L. (Eds.), From Cado-mian Active Margin to the Core of the Variscan Orogen: The pre-Mesozoic Geology of Saxo-Thuringia (NE Bohemian Massif). Schweizerbart'sche Verlagsbuchhandlung, Stuttgart, pp. 195–220.